Clinical and Translational Imaging (2020) 8:243–263
https://doi.org/10.1007/s40336-020-00376-y

EXPERT REVIEW

Towards quantitative small-animal imaging on hybrid PET/CT and PET/MRI systems

Mahsa Amirrashedi[1,2] · Habib Zaidi[3,4,5,6] · Mohammad Reza Ay[1,2]

Received: 7 April 2020 / Accepted: 14 June 2020 / Published online: 23 July 2020

Abstract

Aim Over the past two decades, innovations in small-animal positron emission tomography (PET) have reached an impressive level, which has brought countless opportunities to explore the major puzzles in biomedical research. It is a given that pairing information coming from different imaging modalities renders unprecedented knowledge and provides a great insight into various facets of biological systems, such as anatomy, function, physiology, and metabolism in animal models of human diseases, which are difficult to be beaten by standalone PET scanners. The development of bimodal and tri-modal imaging platforms with advanced software solutions dedicated for quantitative studies in small-animals has spurred academic and industrial interest. However, it is undisputed that the potential success of these scanners in filling the translational gap between human and animal findings, hinges to a great extent upon optimization and standardization of relevant parameters and acquisition protocols, which is often overlooked.

Methods This article reviews the trends till 2020 in the field of preclinical PET imaging with emphasize on image reconstruction and quantitative corrections implemented on state-of-the-heart hybrid systems. First, the challenges, limitations, and benefits offered by multi-modality imaging systems are described and then, the most commonly used strategies, as well as novel techniques for image reconstruction and image corrections (attenuation, scattering, normalization, motion, and partial volume effect) are presented. The advantages and disadvantages of different methods are also discussed. We also briefly touch upon the factors that should be considered for reliable kinetic modeling and absolute quantitation in preclinical small animal research.

Conclusions Multi-modality imaging has attracted a lot of research, particularly in the preclinical portfolio. Nevertheless, more research is still needed to optimize the conceptual design, reach the limits of quantitative imaging and implement standardized protocols for small-animal studies. Without any doubt, exploring the potential advantages of combined imaging units providing optimal image quality and reliable tools for quantification of biological parameters through standardized imaging protocols is one of the goals of translational research.

Keywords Preclinical imaging · Image reconstruction · Kinetic modeling · Multi-modality · Quantification

✉ Habib Zaidi
habib.zaidi@hcuge.ch

✉ Mohammad Reza Ay
mohammadreza_ay@sina.tums.ac.ir

[1] Department of Medical Physics and Biomedical Engineering, Tehran University of Medical Sciences, Tehran, Iran

[2] Research Center for Molecular and Cellular Imaging, Tehran University of Medical Sciences, Tehran, Iran

[3] Division of Nuclear Medicine and Molecular Imaging, Geneva University Hospital, 1211 Geneva, Switzerland

[4] Geneva University Neurocenter, Geneva University, 1205 Geneva, Switzerland

[5] Department of Nuclear Medicine and Molecular Imaging, University of Groningen, University Medical Center Groningen, 9700 RB Groningen, Netherlands

[6] Department of Nuclear Medicine, University of Southern Denmark, 500 Odense, Denmark

Introduction

As one of the most ubiquitous and versatile tools in investigations involving laboratory animals, preclinical PET scanners are gaining more ground and growing tremendously in various fields of biomedical research [1]. To tackle the difficulties faced by stand-alone PET scanners, particularly in the context of quantitative imaging capabilities, most of the recent advances focused on the development of multi-modality imaging units to provide unparalleled understanding of the various facets of biological systems, such as anatomy, function, physiology, and metabolism in animal models of human disease [2]. This has spurred academic and industrial interest in developing bimodal and tri-modal imaging systems supported with advanced software solutions to enable quantitative studies in small-animals. However, it is undisputed that the potential success of these scanners in filling the translational gap between human and animal findings hinges to a great extent upon optimization and standardization of the relevant parameters and acquisition protocols which is often overlooked. In this review, state-of-the-art multi-modality imaging systems dedicated for murine studies are described. Special attention is paid to reconstruction methods and quantitative corrections as applied to hybrid preclinical PET scanners. The advantages and drawbacks of the different approaches are also discussed. We also briefly touch upon the factors that should be considered for reliable kinetic modeling and absolute quantification in preclinical studies.

Multimodality imaging: challenges, benefits and pitfalls

The introduction of multi-modality imaging systems opens up a new avenue in healthcare to improve interpretation accuracy by correlating anatomical, functional and morphological information extracted from different imaging units. The majority of small-animal imaging devices were developed as stand-alone PET scanners with many of them being upgradable to multi-modality imaging platforms to tailor the system to different high-level task-based applications. These platforms combine PET scanners with other modalities, such as CT (e.g. IRIS [3], G8 [4], GNEXT [5], NanoScan PET/CT [6], Bruker PET/CT Si78 [7]), SPECT (e.g. VECTor [8, 9], YAP(S)PET [10]), X-ray (e.g. G4 [11]), MRI (e.g. NanoScan PET/MRI [12], MRS-PET [13], Bruker PET inline [7]) or optical imaging (OI) (e.g. VECTor^{4}CT [9]). In addition, a number of commercial tri-modality PET/SPECT/CT systems were also available on the market, including Siemens Inveon [14], Gamma Medica Triumph, MILabs VECTor^{6}CT [9], Bruker Albira [7, 15] and Mediso NanoScan [16]. Beyond dual- and tri-modality units, MILabs VECTor platform extends its usage and applications by combining four imaging modalities PET/SPECT/OI/CT with different strengths and capabilities in a single device [9].

Multimodality imaging is achievable by translating a dedicated animal bed through separate units, docking models or fully integrated platforms. Among all combinations, PET/CT scanners are the most straightforward and reliable hybrid designs available in the preclinical market. Besides providing a high-resolution anatomical reference for PET images, CT enables object-specific quantitative corrections which is the unbeatable advantage of the PET/CT over other integration modes. Apart from numerous benefits offered by combined units, there are still several challenges lying in merging different modalities in a single platform, the most important being is the cross-modal registration of several datasets to ensure precise spatial consistency in different parts of the animal's body. Scanners with off-line image registration are more prone to positioning and motion errors caused during the translation, attachment and detachment of the animal chamber between separate units. Therefore, designing portable and fully compatible animal beds equipped with fiducial markers could be a promising solution for neat alignment in such designs. To this end, most of the marketed scanners are supplied with specific animal supports. A prime example of this are the MOLECUBES series [17], commercialized as three individual imaging units for SPECT (γ-CUBE), PET (β-CUBE) and CT(X-CUBE) in small footprints; any offline combination of PET, SPECT and CT are all feasible via a multi-modal special chamber that is well-suited to each of the scanners [18]. Capillary cells filled with radioactivity are used as registration aids to derive transformation matrices among the three scanners. In the SOFIE G8 PET/CT, a 3D fillable grid was implemented to generate a more accurate transmission matrix [4]. Dedicated chambers were also adopted in other integrated platforms, such as the Mediso NanoScan families [16]. This company provides a range of in-line multi-modality solutions as well as a variety of specific MultiCell imaging chambers compatible with mouse, rat, rabbit and multiple rodent chambers to obtain a higher throughput [16]. Some of these dedicated animal assemblies are shown in Fig. 1.

A number of coplanar preclinical PET/CT scanners combining partial-ring PET with CT to perform simultaneous PET/CT imaging were also developed. The first coplanar design comprising a mini-focal X-ray tube and amorphous selenium flat panel X-ray detector and LSO-based planar detector modules coupled to PS-PMTs was developed by Goertzen et al. for simultaneous mouse imaging [19]. Another design is the ClearPET/XPAD prototype model

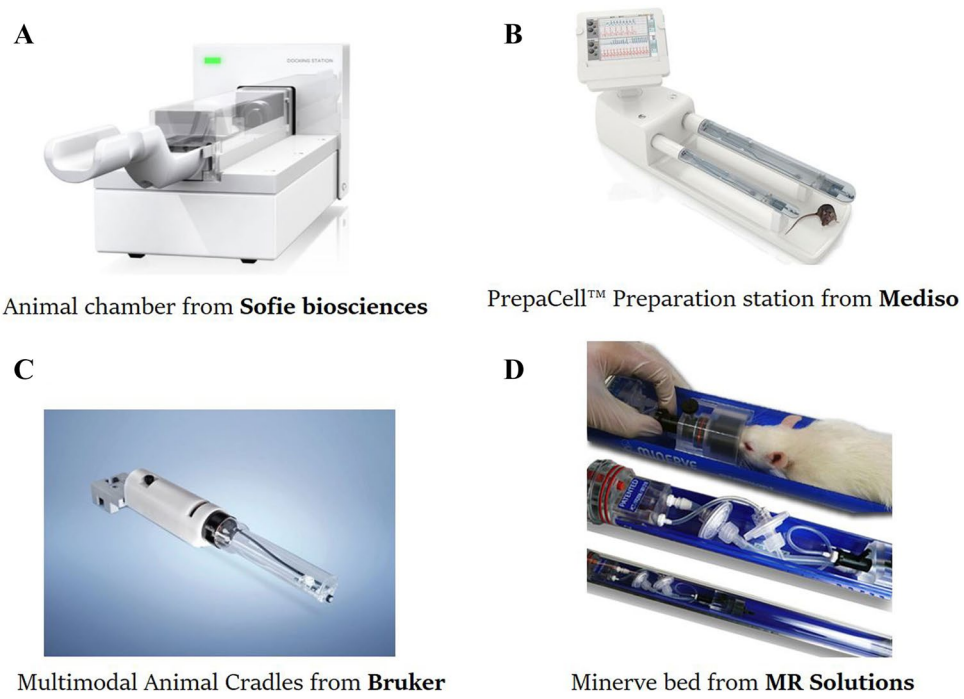

Fig. 1 Dedicated animal assemblies available from different commercial companies. Courtesy of the listed companies

[20] combining the ClearPET LSO/LuYAP phoswich detection modules with the XPAD3 hybrid pixel X-ray detector together placed on a rotating gantry and sharing the same FOV. The PET detector modules were shielded with 150 µm lead to decrease the effect of low-energy X-ray photons while preserving enough detection capability to detect 511 keV photons [20]. Other coplanar designs like VrPET/CT [21] and rPET-1 [22] were also commercialized. Besides seamless co-registration, fast workflow, and high throughput, simultaneous multimodality imaging permits the screening of abrupt alterations in the biological status of the body just with a single dose of anesthetic agents.

Another revolution in preclinical imaging arena emerged by combining PET and MR imaging modalities inspired by successful applications of PET/CT combination. The preclinical applications of PET/MRI imagers in different fields, including neurology, cardiology and oncology were comprehensively reviewed by Judenhofer and Cherry [23]. There are several unique advantages offered by PET/MRI workflows, including lack of ionizing radiation, superb soft-tissue contrast, highly flexible MRI sequences and multiparametric nature of this imaging modality, providing functional along with anatomical information suitable for motion and partial volume effect (PVE) compensation, which are difficult or even impossible to achieve with other combined devices. However, the integration of PET and MRI technologies is technically more challenging in comparison to other hybrid units [24, 25]. Unlike CT, MRI fails to provide an accurate attenuation map for quantitative corrections in PET. Since the attenuation effect is not critical in small-animals imaging, it has been shown that a dual-compartment segmentation-based method gives promising results using the NanoScan PET/MRI preclinical scanner [12]. The second problem is inter-modality interference between PET and MRI components, which limits the performance of PET system in the presence of MRI magnetic fields and vice versa. So far, efforts have been focused on addressing this issue through various strategies, including designing PET/MRI systems using long optical fibers to keep the PMTs/electronics far away from the MR magnetic field [26], shielding the PMTs/electronic or modifying MRI subcomponents and devising MRI-compatible readout electronics [7]. The first concept was pursued by several vendors, including the NanoScan PET/MRI [12], Bruker's PET inline scanners [7] and PET clip-on from MR Solutions [27]. The NanoScan PET/MR utilizes LYSO/PSPMT detectors placed linearly with a 3 T cryogen-free magnet or 1 T permanent magnet. PET/MRI inline composed of monolithic LYSO/SiPM detectors (known as Si detectors) compatible with a great range of MRI scanners. Another unique design belongs to PET clip-on from MR Solutions which could be attached to either MRI or CT units. Contrary to PET/CT scanners performed commonly in sequential configurations, PET/MRI can be aligned in either sequential or simultaneous modes. The sequential mode simplifies the technical integration of the systems on the one hand while increasing the co-registration uncertainty on the other. Commercially marketed PET inserts along with inline PET/MRI scanners are shown in Fig. 2.

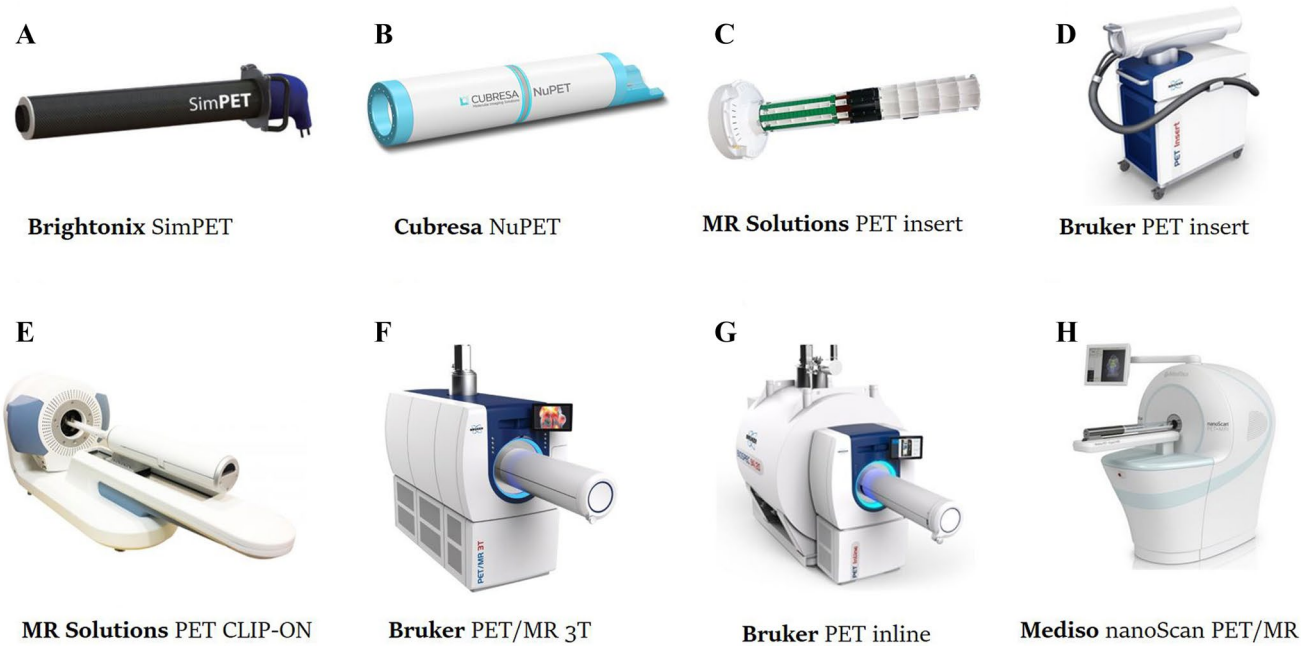

Fig. 2 Commercially available dedicated simultaneous (top row) and sequential (bottom row) preclinical PET/MRI instruments. Courtesy of the listed companies

Rapid advancements in readout electronics and the introduction of MR-compatible photodiodes (e.g. solid-state avalanche photodiodes (APDs), analog/digital Silicon PMTs—SiPMs) facilitate the commercialization and availability of fully integrated PET/MRI technology as reviewed recently by Lee et al. [28]. Among the available hybrid imaging systems, simultaneous PET/MRI inserts occupied major interest in preclinical trials owing to their ultra-compact configuration, easy installation and relatively lower design cost [7, 28–36]. MR Solutions offers an innovative PET insert compatible with MRI up to 9.4 T, for which the PET ring is made up of dual-layered LSO crystals read out by SiPMs [13]. Another compact and unique detector arrangement belongs to MADPET4 which allows fitting within a 7 T Agilent-Bruker BioSpec 70/30 MRI scanner [34]. The insert incorporated dual-layered LYSO arrays with one-to-one coupling to SiPMs. A similar design based on dual-layered LYSO/SiPM detector blocks was reported by Goertzen et al., which is capable to operate inside high-field MRI systems, such as 70/20 and 94/20 models of the Bruker BioSpec [30] and introduced to the market as Cubresa's NuPET in-bore PET [38]. In 2019, Cubresa introduced a new member of the NuPET family, designed specifically for non-human primate imaging, which could be used within clinical scanners [38]. Another LYSO/SiPM detector ring intended to be placed inside the 7 T preclinical MRI was the PET insert presented by Ko et al. which is now commercialized through Brightonix as Sim-PET families with different transaxial and axial fields-of-views (FOVs) [39, 40].

Hyperion Π^D is a highly integrable PET/MRI insert thanks to its fully digital design using SiPMs in which the digital signals are directly produced within the microcells [35]. Compared to other inserts, Hyperion Π^D has a larger bore diameter (209 mm) and axial length (96.6 mm) with submillimeter crystal dimensions and minimum interference between PET and MRI sub-units [35]. Bruker recently offered commercial PET inserts with continuous crystals and SiPM readout compatible with high-field MRI systems up to 15.2 T [7]. The PET component of Bruker's inserts features the same technical specifications mentioned above for PET inline unit.

MRI-compatible HALO 3.0 (bore size ~ 75 mm) and HALO 2.5 (bore size ~ 65 mm) inserts for rodent imaging are now commercially available from Inviscan SAS. These inserts are produced in 40 and 80 mm axial extensions with 5% peak sensitivity (with 80 mm AFOV) and 1.1 mm spatial resolution [41]. Technical specifications of PET/MRI scanners designed for preclinical research are summarized in Table 1.

Combining two functional imaging techniques, such as PET/SPECT and PET/OI, is one of the, if not the most important, trends toward hybrid imagers which traces its roots to the successful fusion of anatomical/functional images. The YAP(S)PET was the first commercial unit that enabled concurrent PET/SPECT through four rotating detector heads based on YAP:Ce matrices [10]. For hybrid imaging, one detection pair detects annihilation photons in coincidence mode while the second enables single-photon

Table 1 Technical properties of commercial PET/MRI scanners dedicated for preclinical studies

Scanner	Integration mode	Company	Detector	Crystal size (mm^3)	TFOV[a]	AFOV[a]	Sensitivity	Spatial resolutio[n,b] (reconstruction method)
PET/MR 3 T [7]	Sequential	Bruker Bio-Spin	Si detectors (LYSO/SiPM)	Monolithic	80	~150	12%	0.7 (MLEM)
PET-inline [7]								
PET insert [7]	Simultaneous							
SimPET-S [40]	Simultaneous	Brightonix	Dual layered LYSO/SiPM	1.2×1.2×10	60	55	NA	0.7 (3DOSEM)
SimPET-X					60	110		
SimPET-L					76	55		
SimPET-XL					76	110		
NuPET [38]	Simultaneous	Cubresa	Dual layered LYSO/SiPM	1.2×1.2×6 1.2×1.2×4	59	67	5.5%	1.3 (FBP) 0.9 (MLEM + PSF)
PET insert 40 [13]	Simultaneous	MR Solutions	Dual layered LYSO/SiPM	1.6×1.6×6 1.6×1.6×4	40	50.20 (1 ring) 102.48 (2 rings) 151.2 (3 rings)	NA	<0.8 (3DOSEM)
PET insert 80					80			
PET CLIP-ON 80 series [13]	Sequential				80			
PET CLIP-ON 120 series					120			
NanoScan PET/MRI [12, 16]	Sequential	Mediso	LYSO/PSPMT	1.12×1.12×13	120	100	8%	0.7 (3DOSEM) 1.25 (FBP)
HALO 3.0 [41]	Simultaneous	Inviscan	SiPM based detectors	NA	75	40 (1 ring) 80 (2 rings)	5% (1 ring)	1.1 (NA)
HALO 2.5					65			

NA not available

[a]All values expressed in mm

[b]Spatial resolution at the center of the scanner

acquisition by means of lead collimators. Another joint PET/SPECT platform with stationary full-ring gantry was developed by MILabs. The scanner termed VECTor is the only one in the market today that shares the same detector modules to capture single photons emanating from either PET or SPECT tracers by incorporating clusters of pinholes with small acceptance angles placed on each detection head [8]. It is also possible to derive information-rich PET/SPECT/Optical images through an upgraded version of the VECTor by adding MILabs' dedicated optical imaging unit on the VECTor platform [9]. Few research groups reported on devising PET/OI hybrid scanners [42–44]. OPET is the first prototype developed at the University of California Los Angeles (UCLA) for simultaneous PET and Bioluminescence imaging [45]. OPET is composed of six detection modules based on BGO crystals coupled to a multi-channel PMT forming a 35-mm ring diameter. The scintillation arrays are used as optical fibers to guide bioluminescence photons toward photosensors.

Overview of advanced image reconstruction techniques

Advances in image reconstruction are often accompanied by the burst of incremental innovations in hardware components and scanner architecture, which is mainly invigorated by demands for higher image quality and more accurate quantitative analysis. Image quality achieved in PET imaging is dictated by a number of attributes, including scanner performance, injected dose, acquisition parameters and reconstruction algorithm. However, the role of animal handling and preparation cannot be underestimated in preclinical setting [46].

There are two general classes of algorithms used to estimate the three-dimensional (3D) distribution of radiolabeled compounds from the coincidence events detected by a PET scanner, namely (1) analytical and (2) statistically iterative reconstruction methods [47, 48]. Filtered

backprojection (FBP) was the most popular mathematical framework during the early developments of nuclear medicine instrumentation, which is based on analytical inversion formula that overlooks the inherent uncertainties in PET imaging, including the stochastic nature of PET data, positron decay process, the adverse effects of attenuation, Compton scattering, random events and the photon detection chain. As such, the produced images suffered from less than optimal noise properties and quantitative inaccuracies. The 3D reprojection (3DRP) algorithm was widely adopted for fully 3D PET image reconstruction [49]. Even though analytic methods are very fast, easy to implement and straightforward, the noisy nature of the final image stimulated the substitution of these strategies by more efficient iterative statistical techniques. Of all iterative algorithms proposed for PET imaging, Maximum Likelihood Expectation Maximization (MLEM) [50], its accelerated version called Ordered Subsets Expectation Maximization algorithm (OSEM) [51] and maximum a posteriori (MAP) [52] gained widespread acceptance and have been used for image reconstruction on preclinical PET scanners. Even though 3D reconstruction guarantees better resolution in the axial direction, a number of companies have also implemented 3D to 2D rebinning methods (e.g., SSRB [53], FORE [54], MSRB [55], FORE-X [56], FORE-J [57], AFORE [58]) followed by 2D reconstruction when fast reconstruction was desired [54]. For small axial extensions (axial fan angle $\leq 20°$), the results of 2D methods might be promising but seem to fail for larger AFOVs owing to uncertainties associated with rebinning methods [58, 60].

The slow convergence rate associated with MLEM algorithms led to the emergence of block iterative methods, such as OSEM in emission tomography. However, increasing the number of subsets in OSEM to achieve full convergence results in noisy images. The problem is conventionally addressed by early termination of the algorithm or post-smoothing, which in turn compromises the quantitative accuracy of the resultant image. Whilst most scanners are operated with MLEM or OSEM, significant efforts were devoted to developing more advanced algorithms [52].

One of the most attractive and frequently used algorithms in preclinical PET studies is penalized maximum likelihood (PML) or MAP which produces fairly uniform images without incrementing sharp features and jeopardizing the final image when using a high number of iterations. The amount of smoothing in the MAP algorithm is heavily managed through the regularizing effect of a prior term [52]. Incorporating structural side-information available on hybrid systems as a prior within the MAP framework results in images with improved noise properties, higher spatial resolution and better edge-preservation. This could be achieved for example by utilizing higher priors within the boundaries defined by a segmented CT or MR image [61], or increasing the smoothing among adjacent voxels with approximately similar CT or MRI intensities [62].

Other regularized methods incorporating relaxation parameters to control image noise, such as row action maximum likelihood algorithm (3D-RAMLA), have been adopted and incorporated in the early generation of preclinical PET scanners, such as the Mosaic HP [68]. The modified version of RAMLA with an improved convergence rate, called dynamic RAMLA or DRAMA, has been introduced by Tanaka and colleagues and extended for various applications [69]. This algorithm is used as the main reconstruction method on the ClairvivoPET small animal scanner [60]. DRAMA utilizes a subset-dependent relaxation parameter regarding system geometry to suppress noise amplification in each subset. Image quality measurements on the ClairvivoPET scanner indicate that one pass DRAMA results in lower noise and higher RC values in contrast to other methods [60]. The uniformity achieved by list-DRAMA with the ClairvivoPET scanner was threefold better than the one achieved by the FBP algorithm. In the realm of commercially available state-of-the-art preclinical PET scanners, the Tera-Tomo reconstruction package adapted to Mediso NanoScan family is one of the notable examples employing a tunable regularization approach using a total variation (TV) term in 3D OSEM reconstruction to generate more uniform images compared to other preclinical PET scanners [6, 12]. In addition, it should be emphasized that other physical effects, such as positron decay, attenuation, scattering, and detector response are all incorporated in the Tera-Tomo engine as well. The effect of these factors on image quality will be discussed in the following sections below.

Recently, the impetus grows to seek other types of regularized EM methods with more adaptive subsettings like Statistically Regulated EM (StatREM), Pixel-based OSEM (POSEM) and Count-Regulated OSEM (CROSEM) [70, 71]. These types of algorithms, extensively used in SPECT, lead to improved spatial resolution in high-count regions while reducing the noise level in low-count regions by incorporating wise statistical tests in the reconstruction chain. POSEM was adopted on the MILabs VECTor, a simultaneous SPECT/PET scanner with a different design concept [8, 72].

Optimizing image reconstruction parameters for different imaging scenarios is one of the most important tasks following PET scanner performance evaluation using International standards. Factors reported to be influencing image quality have been explored in few studies [58, 73]. These evaluations emphasized that achieving the desired image quality and quantitative accuracy requires the optimization of reconstruction algorithms and tuning the post-processing parameters depending on the imaging tasks.

Resolution recovery image reconstruction

A number of compounding factors impair the spatial resolution in PET imaging. These are of utmost importance in preclinical studies owing to small and tiny structures within the rodents. Although the spatial resolution is considered during the conceptual design of preclinical PET devices (e.g., by incorporating minuscule detector elements with depth-of-interaction (r) capability, one-to-one crystal-to-SiPM coupling, etc.), other contributory factors should be considered within the reconstruction process to fully exploit advantages of the hardware.

As mentioned earlier, major benefits can be achieved through iterative reconstruction scheme owing to their capability in modeling the physics of PET imaging within the so-called system response matrix (SRM) through resolution recovery image reconstruction [74]. Moreover, quantitative corrections including normalization, attenuation, scattering, random, as well as motion, can be modelled within the reconstruction framework to preserve the statistical properties of the data in a more efficient manner. Therefore, the accuracy of the system model is the most crucial factor in iterative reconstruction underpinning the quality of PET images by defining the most realistic relation between acquired projection data and reconstructed images [75]. Surveys such as that the one conducted by Wang et al. showed that incorporating the system model into the 3D OSEM algorithm improves the recovered spatial resolution by a factor of 20% on the dedicated small animal Argus PET scanner [76]. 3D OSEM reconstruction incorporating detector response modeling considering both depth of interaction and scattering within the crystals in the NanoScan PET/CT and PET/MRI scanners translated into obvious improvements and higher signal-noise-ratio (SNR) compared to approximate methods that ignore intercrystal scattering [12, 77].

In this vein, one could combine all resolution degrading factors in a unified detection probability matrix (P) or model them separately in a factorized fashion to tackle the excessive cost and computational burden [78]. Typically, the SRM is decomposed into several components [52]:

$$P = P_{\text{att}} \cdot P_{\text{norm}} \cdot P_{\text{positron}} \cdot P_{\text{detector}} \cdot P_{\text{geo}}, \quad (1)$$

$P \epsilon \mathbb{R}^{M \times N}$ is the detection probability matrix defining the probability of a photon emitted from voxel n being detected in detector pair m. $P_{\text{att}}$and$P_{\text{norm}} \epsilon \mathbb{R}^{M \times M}$ are diagonal matrices including attenuation and normalization coefficients, respectively. $P_{\text{positron}} \epsilon \mathbb{R}^{N \times N}$ represents the positron range effects. Annihilation pair non-collinearity, penetration and inter-crystal scattering are all included in $P_{\text{detector}} \epsilon \mathbb{R}^{M \times M}$. P_{detector} is also called the sinogram blurring matrix. Lastly, the geometric relation between voxel n and detector pair m is modeled in $P_{\text{geo}} \epsilon \mathbb{R}^{M \times N}$, where P_{geo} as the core ingredient in the system matrix. This may be calculated through Siddon, accelerated Siddon, trilinear interpolation, angle subtended, Wu-antialiased or other techniques [75].

Different strategies were followed for modeling the detector response function, including experimental (direct) methods, Monte-Carlo (MC)-based system modeling and analytical approaches. These methods have also been applied on current preclinical PET devices. A comprehensive review about system modeling in iterative image reconstruction is given by Iriarte et al. [75]. Briefly, in direct measurements, the overall system response model is determined through scanning of a precisely aligned small point source or a line source at each voxel position [79]. Although the method is elaborate and lengthy, it derives the most accurate SRM by considering the real scanner's geometry [79]. One may estimate an approximate SRM from a sampled set of point source measurements. For example, in the MiniEXPLORER II designed for whole-body large animal imaging, the SRM is extracted by scanning a point source through a 3D robotic stage at 6862 transaxial positions at the central slice of the scanner [80]. It should be noted that the choice of the appropriate method to be used for SRM modeling is strongly influenced by the scanner geometry and design complexity. Since the dimensions of the SRM depend directly upon the number of detector pairs and image dimensions, in the majority of state-of-the-art high-resolution preclinical PET scanners consisting of a large number of small detectors and incorporating finer reconstruction grids, MC simulations and hybrid methods are becoming more prevalent. To this end, several strategies were adopted to decrease the simulation time and SRM dimensions by taking into account the sparseness and possible geometrical symmetries. For the first-generation Sherbrooke small-animal PET, a compression factor of 512 was achieved by exploiting the 512 symmetries both in the axial and transaxial directions [81]. Considering the cylindrical symmetries of the MADPET-II scanner, 72 cylindrical symmetries were reported [82]. Recently, a general algorithm called symmetry search algorithm was proposed to automatically depict the geometrical symmetries in various scanners, leading to higher compression factors compared to conventional methods [83]. One of the most distinctive approaches to compress the prohibitive size of the SRM with multi-layered crystals with DOI capability was suggested by Li et al., in which the DOI information from all layers was summarized in a smaller virtual ring around the object, leading to a drastic reduction in SRM dimension by a factor of 2×10^7 [84].

MC generated SRM has also been in use by a number of major preclinical PET instrumentation vendors to achieve a uniform and homogeneous spatial resolution across the FOV. Accurate SRM modeling through MC simulations has been shown to eliminate parallax errors toward the edge of the FOV in the Trans-PET scanner [85]. In the MADPET4

small-animal PET insert with dual-layered LYSO detectors, MC-based SRM results in highly uniform spatial resolution all over the transaxial FOV [34]. In the Tera-Tomo reconstruction engine, MC generated SRM implemented on graphics processing units (GPU) resulted in noticeable improvement of noise properties and increased the homogeneity of the SNR phantom [16]. In contrast, in the YAP(S) PET [10] and IRIS-PET [3], a hybrid method was employed to derive the SRM where Siddon-based multi-ray tracing with Gaussian integration weights were utilized to calculate the geometric matrix and crystal depth effect, while inter-crystal scattering was modeled through simulations [86]. The analytical multi-ray tracing approach was also applied on the MRS-PET insert [13]. For MILabs' VECTor, a somewhat different methodology was followed for generating the system response function for the particular pinhole collimation geometry of the system [72]. The scanner employs clustered pinhole collimators on three NaI(Tl) detectors configured in a triangular fashion enabling simultaneous SPECT and PET imaging acquisition modes based on single photon detection. For SPECT reconstruction, a set of experimental measurements using a point source was used to derive the system matrix owing to uniform absorption of low-energy photons on the detector surface. Conversely, the reconstruction of pinhole PET images utilizes a depth-dependent system matrix generated by taking into account the attenuation of photons in the pinhole collimator and crystal. The results of phantom studies indicated a good recovery by including variable DOI during iterative reconstruction [72].

It has amply been pinpointed that image quality and quantitative accuracy in the new generation preclinical PET scanners with submillimetric spatial resolution are likely to be deteriorated by positron range [59, 87, 88]. The effect becomes more relevant for high-energy positron-emitters with long positron range (> 1 mm), such as ^{13}N, ^{15}O, ^{68}Ga, ^{66}Ga, ^{82}Rb and ^{124}I. Higher SORs and smaller RCs were reported for high-energy radioisotopes [89]. Different strategies were assessed to recover the resolution loss caused by the positron range effect. Overall, positron blurring kernel (obtained through analytic calculations or MC modelling) could be (1) handled in the forward projection of the reconstruction algorithm or (2) accurately modelled in the SRM as shown in Eq. 1 [90, 91]. The former was investigated by Gonzalez et al. [92] on the Argus PET scanner and the latter was deployed on the MicroPET-R4 scanner [93]. In both studies, clear improvements in image quality and quantitative accuracy following positron range correction were reported.

Moreover, it has been demonstrated that positron range effect depends significantly upon the physical properties of the medium and surrounding tissues. This has spurred the interest towards more accurate methods like CT-based tissue-dependent spatially-variant models which ultimately render artifact-free images, improved quality and better tumor delineation when using high-energy radioisotopes such as ^{68}Ga [87, 94].

In this context, particular attention should be paid to positron range correction on simultaneous PET/MRI systems where the effect of magnetic field on the positron distribution is measurable. As reported in a number of studies, the Lorentz force generated in the presence of magnetic field limits the positron trajectories in the transaxial plane, consequently improving in-plane spatial resolution [90, 95]. Since this is not the case in the axial direction, this phenomenon results in a non-isotropic positron range effect or so-called shine-through artifact. Hence considerable attention should be paid to modeling the non-uniform positron range-effect in PET/MRI systems, particularly for high-energy positron emitters [96].

4D Image reconstruction methods

With the emergence of dynamic PET data acquisition which provides a great insight into dynamics processes underlying the tracer distribution, the focus of attention shifted toward 4D iterative reconstruction methods [63, 64]. Information about tracer kinetics could be gathered through a sequence of contiguous PET frames. To obtain the desired pharmacokinetic parameters, one would like to reconstruct the 2D or 3D activity distribution in each frame separately and then estimate the functional parameter by fitting a suitable model to the time–activity curve (TAC) in each voxel or region-of-interest (ROI). This method is referred to as indirect kinetic parameter estimation. The main drawback associated with conventional 3D indirect reconstruction is the limited number of counts in each frame, which ultimately introduces a great level of bias in kinetic parameters derived from noisy TACs, particularly when voxel-wise methods are applied. This issue is more pronounced for short-lived radioisotopes as well as small-animal studies where high temporal resolution is needed to handle fast biological timescales of rodents compared to humans [97]. Alternatively, if the kinetic parameters are extracted directly from PET raw data or sinograms and then modeled within the reconstruction task, better noise properties are expected. These direct parametric image reconstruction methods offer prodigious advantages in terms of noise reduction and quantitative accuracy. However, this approach is more sophisticated compared to indirect methods, particularly for nonlinear and complex kinetic models [98]. A broad range of algorithms was deployed in the context of 4D image reconstruction, which were well categorized and covered in previous reviews by Reader et al. and Rahmim et al. [63, 64]. However, much research in this area has focused on using 4D spatiotemporal basis functions or scaling 3D spatial basis

functions with a linear or nonlinear temporal basis functions. Several models were suggested and examined in this vein as comprehensively discussed in [63]. For example, simple basis functions, such as rectangular, wavelet, spline basis functions or physiologically meaningful models like Patlak, Logan, decaying exponential or spectral analysis were used.

Albeit, the feasibility of the 4D reconstruction has been extensively studied in clinical studies, far too little attention has been paid to the quantitative performance of these methods in preclinical research setting. Cheng et al. evaluated the impact of direct and indirect reconstruction methods on the quantification of tumor hypoxia from dynamic ^{18}F-FMISO PET scanning [99]. A better correlation was found for kinetic parameters extracted from direct reconstruction methods (including Patlak graphical model within the OSEM algorithm) using immunohistological assays as physiological reference. Moreover, direct strategies with multi-tracer kinetic models have led to promising results in separating signals of ^{18}F-FLT and ^{18}F-FDG from a single mouse dynamic scan [100].

Another category of 4D or higher dimensional image reconstruction belongs to iterative algorithms including motion compensation to avoid further resolution degradation and artifacts generated by cardiac and respiratory motion [101, 102]. The problem of physiological motion is more pronounced for small structures and high-resolution preclinical scanners in which the spatial resolution of the scanner is lower than the motion's amplitude [103, 104]. Motion-induced inconsistencies in PET imaging could be addressed in two distinct ways: (1) separately reconstructing the gated frames (each frame corresponds to the average or sum of all events in the same phase of the cardiac or respiratory cycle) or (2) implementing motion correction in the iterative reconstruction framework as a unified paradigm. The latter offers an elegant solution with unpreceded advantages in terms of SNR.

Marked enhancements in visual image quality and quantitative parameters were reported following motion correction in small animal studies. For the first time, simultaneous cardiac and respiratory gating in mice PET imaging was reported on the microPET scanner with an overall 1 µl volume resolution. Clear improvements in cardiac images and ejection fraction estimation were reported with cardiac gating, while the effect of respiratory gating was not notable [105]. Similar results were achieved through cardiac gating in conjunction with respiratory gating for mice cardiac scans on the preclinical quadHIDAC scanner [106]. This latter study proved that cardiac-gated FDG images of the mouse heart led to better quantification (smaller wall-thickness, wall-to-wall-separation, and blood-heart-ratio) in comparison to ungated cardiac images while the effect of the respiratory gating was negligible owing to small respiratory amplitude in comparison to the PET scanners' spatial resolution [106]. A novel respiratory gating method was proposed by Todica et al. in which the alterations in the amplitude of the ECG signal and heart-beat variations during the breathing cycle of the rat heart scan have been detected and utilized as respiratory triggered signal to improve quantitative values [107]. Herraiz et al. proposed a data-driven approach for automatic gating in small animal cardiac imaging which involves analyzing the count-rate variation of the heart in the frequency domain [94].

More accurate and robust motion correction using high-resolution anatomical images is gaining more ground following the commercialization of hybrid scanners with sub-millimetric spatial resolution [108, 109]. Preliminary work on MRI-based motion correction in simultaneous PET/MRI was undertaken by Chun et al. [110]. In the proposed method, displacement fields were estimated from tagged MRI using non-rigid registration methods and then embedded into the SRM. The method was used to reconstruct data collected from scanning a phantom, rabbit and non-human primate. Compared to conventional gating methods, the incorporation of MRI-based motion compensation within an iterative framework resulted in higher SNR and substantially improved lesion detectability [110]. Noteworthy, in addition to motion-induced blurring, another major source of uncertainty is the deformation of the attenuation map during respiratory motion, which should be compensated considering the different respiratory phases. Motion-compensated 4D PET reconstruction incorporating motion information and proper attenuation map derived from 4D cone-beam CT in small-animal imaging resulted in smaller errors in tumor volume and standard uptake value (SUV) quantification [111]. In a work similar to Chun et al., the attenuation map of the animal is deformed based on the measured motion field through tagged MRI acquisition and a motion-dependent attenuation map incorporated in the PET reconstruction model [112]. This technique provided higher contrast and the same level of noise in comparison to uncorrected images.

Undoubtedly, the most important issue in this section is linked to imaging conscious or freely moving animals. Routinely, small animal PET imaging is carried out under anesthesia to reduce the likelihood of animal motion during image acquisition. It is well-established that imaging awake and unrestrained animals can provide richer information in brain studies in the absence of anesthesia which might change the brain physiology. To the best of our knowledge, two different mechanisms were adapted to scan awake rodents: (1) The first approach utilize dedicated wearable brain rings and (2) the second compensates gross body motion by the aid of motion tracking devices. Such a design concept was depicted in Fig. 3. Due to the rapid movements of small-animals, motion tracking is more challenging particularly when the animal is agitated and not calm. Zhou et al. deployed an optical motion tracking

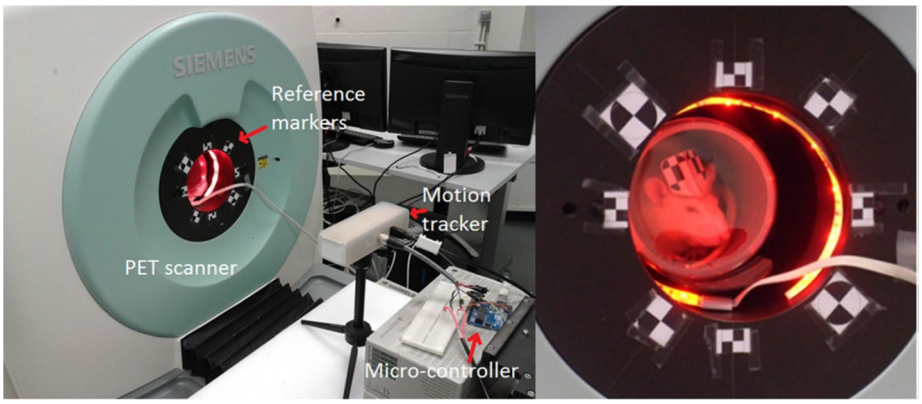

Fig. 3 An example of the set up proposed by Miranda et al. [119] for scanning the awake animal. The Micron Tracker, the microcontroller and reference markers around the Inveon bore, and the illumination for tracking the animal are shown (The figure is licensed under a Creative Commons Attribution 4.0 License)

system along with two check-board markers to obtain the transformation matrix which are to be used for correcting and rebinning the uncorrected LORs before reconstruction [113]. Likewise, Kyme et al. developed marker-based and marker-less motion correction techniques in awake animal imaging and optimized the motion tracking parameters in typical preclinical scenario [114–116]. In a further study by Zhou et al. a dedicated enclosure was devised for imaging freely moving animals and the tracking system was used to capture brain movements of the animal within the chamber [117]. Miranda et al. evaluated the feasibility of marker-less motion tracking using the projected structure stereo camera [118]. It was then demonstrated that motion tracking performs well for gross motion compensation but this procedure alone does not eliminate motion-induced blurring due to the rapid movements of the animal. To compensate for the residual motion error due to the finite frame rate of the tracking system, deconvolution techniques were also implemented [119, 120]. In the most recent paper with Kyme et al., a novel concept, called open-field PET, is introduced [121]. The technique includes advanced motion estimation using optical motion tracking, motion-compensated image reconstruction, a dedicated animal chamber controlled with a 6-axis robotic arm and a special protocol for delivery of the desired tracer/drug to the animal in conscious state.

Advances in quantitative small animal PET imaging

Normalization

Most of the current interest in biomedical sciences and drug development portfolio is centered around quantification of tracer uptake in the animal body. To realize the full advantages of PET imaging in providing quantitative information, a number of corrections must be performed before or within the reconstruction procedure. These include normalization, random smoothing, attenuation, scattering, dead-time, decay compensation, motion correction and scanner calibration. Normalization is the prime correction in PET scanners which cancels out the high-frequency variations reflecting sensitivity variability and geometric factors among different LORs joining opposite crystals. Three common normalization techniques were implemented on preclinical PET scanners: (1) direct normalization, (2) component-based and (3) self-normalization. In the case of the direct method, the normalization coefficient (NC) for each LOR is inversely proportional to the number of counts acquired by scanning a homogeneous and well-centered cylindrical phantom for several hours. Component-based normalization (CBN) is a well-established approach applied in small-animal PET scanners owing to sufficient statistical accuracy. CBN is based on determining and calculating factors affecting LOR sensitivity, such as intrinsic detector efficiencies, block-related parameters, geometrical factors, and time and spatial misalignments separately. Normalization factors could be calculated using a rotating source, uniform plane source, as well as a uniform cylindrical phantom. Self-normalization is another option where the NCs are extracted solely from the PET emission data without the need for extra normalization measurements [122–124]. In this method, it is assumed that the count distribution in an arbitrary PET scan is the product of two distinct components. The low-frequency component is related to activity distribution within the scanned object, whereas the high-frequency component reflects efficiency variations of the scintillation detectors. Hence, by removing the object-dependent count distribution, one could obtain NCs from the emission count map. In a method proposed by Zhang et al., the low-frequency component is derived through three different algorithms (a low-pass filter, local average filter and surface-fitting). The detector efficiency map is then obtained by normalizing the total detector counts with the object-dependent distribution [124]. As for clinical scanners, regular normalization is essential to guarantee accurate and artifact-free measurements in small-animal studies [125].

Strategies for attenuation correction

Notwithstanding the deleterious effects of attenuation and scattering are less significant in small rodents compared to clinical imaging, compensating these errors is a prerequisite for quantitative small-animal imaging. Even though photon attenuation is often neglected in small-animal imaging (particularly in mice), it has received much attention in recent years, particularly with the emergence of combined imaging units tailored for laboratory animal studies. A number of studies investigated the importance of photon attenuation in preclinical setting [126–133]. In a study by D'Ambrosio et al., a 20% SUV underestimation in uncorrected PET images of the nude mouse was reported [130]. These findings were confirmed by another study which reported recovery of tracer uptake of 20% for mice and 40% for rat-sized phantoms following attenuation correction [126]. Likewise, Hayakawa and colleagues assessed the impact of attenuation in cardiac rat imaging and observed an approximate loss of 44% in tracer uptake recovery in obese rats [133].

So far, various approaches have been examined to achieve attenuation-corrected PET images. These techniques fall into two general categories: (1) transmission-less and (2) transmission-based methods [129]. Transmission-based methods rely on an external source (radionuclide source or X-rays) to provide object-specific attenuation map, whereas transmission-less methods estimate uses the emission image of the object to delineate the internal organs boundaries and external body contour followed by assignment of appropriate attenuation coefficients to different tissue classes. Undoubtedly, the most simplified transmission-less method is uniform AC, in which a uniform attenuation coefficient is assigned to a cylinder mimicking the contour of the animal body or the object under study. This method was reported to lead to an overestimation of attenuation coefficients [129, 130].

CT is likely the most appropriate method available today on combined PET/CT systems and is often considered the gold standard technique for assessing alternative techniques. Despite the well-established advantages of providing detailed structural information with lower statistical noise in shorter scan time, there are several issues associated with CT-based methods, such as exposure of the animal to ionizing radiation, potential CT artifacts and sensitivity to co-registration inaccuracies. Furthermore, it is worth bearing in mind that energy scaling is mandatory when using CT or transmission source with energies other than 511 keV, such as ^{137}Cs which emits a gamma ray at 662 keV. Various strategies were devised to convert CT values to attenuation coefficients at 511 keV, including scaling, segmentation, hybrid, bilinear scaling and dual-energy decomposition techniques. The implementation of CT-based AC involved a number of steps summarized in Fig. 4. Prasad et al. implemented CT-based AC on the FLEX Triumph PET/CT and assessed the accuracy of bilinear and quadratic energy-mapping techniques on quantitative analysis of mice and rat PET images [127]. No significant difference was observed between both methods for soft tissues, while small improvements were observed for high-atomic number regions, such as bone when using the quadratic energy scaling [127].

On the early generation standalone PET scanners, such as the microPET-P4, R4 and focus120, a customized rotating ^{68}Ge source was implemented for either normalization or attenuation correction, which enabled transmission scanning in single or coincidence mode. Similarly, a number of commercial preclinical PET scanners used a ^{137}Cs transmission source (e.g. ClairvivoPET [134] and Eplus-60 [135]) or ^{57}Co (e.g. Inveon DPET) [136]. The most important limitation associated with external transmission sources is the noisy nature of the transmission images propagates to attenuation-corrected PET images. Around 4% increase in image noise was observed after implementing radionuclide transmission-based AC using a ^{68}Ge point source on a rat-like phantom [129]. Chow et al. studied the influence of acquisition parameters, including the activity and radius of ^{68}Ge point source, acquisition mode and scan time on noise properties of attenuation-corrected images acquired by the microPET-P4 scanner [128]. They reported marked improvements in SNR of the corrected images when using a higher activity transmission source with smaller rotation radius and single acquisition mode. However, activities higher than 2 mci result in significant artifacts generated by dead-time of the detectors [128].

Nai et al. investigated different approaches for attenuation correction for the ClairvivoPET scanner, including uniform fitting of a cylindrical contour for AC, segmented emission-based and segmented transmission-based AC using a ^{137}Cs source [137]. The uniform cylindrical method outperformed the other techniques for the cylindrical phantom but failed for non-uniform objects like animals. In addition, it was shown that the performance of the emission-based method is highly dependent on the administered radiotracer [137].

D'Ambrosio et al. investigated the performance of CT-based and segmented emission-based AC on the eXplore Vista PET scanner using various phantoms and rodent studies [126]. The accuracy of each method was then evaluated for different radiotracers, including ^{18}F-FDG, ^{11}C-acetate, ^{68} Ga-chloride and ^{18}F-NaF. For phantom studies, the discrepancy between two AC methods was negligible while the accuracy of emission-based method was poor for specific radiotracers, such as ^{18}F-NaF [126].

For the PETbox prototype, two transmission-less methods were adopted and tested using a simulation study [138]. Two VGA video cameras were mounted on top and lateral side of the scanner. The coronal and sagittal views of the object captured by the cameras were replicated and

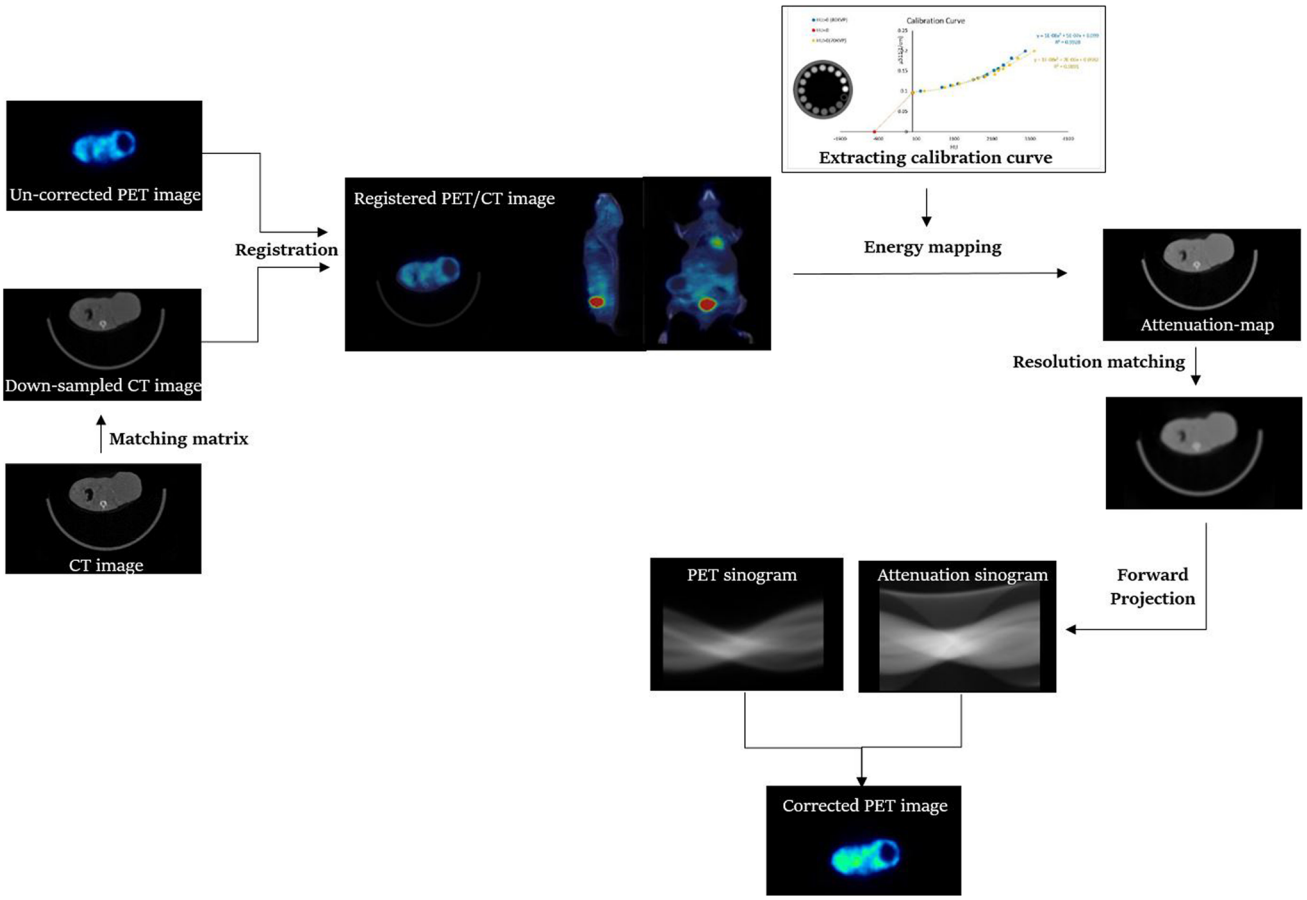

Fig. 4 Principle of CT-based attenuation correction in small-animal PET studies. Similar to clinical PET/CT scanners, CT-based AC include the following steps: (1) down sampling of CT images to match the PET image matrix, (2) registration and re-slicing, (3) energy conversion by means of a calibration curve, (4) resolution matching through smoothing the CT images using a Gaussian filter, (5) forward projection of the attenuation map to get attenuation correction factors, (6) multiply the PET sinograms with corresponding attenuation sinograms to obtain corrected PET images. All the steps shown in Fig. 4 are implemented on Xtrim-PET scanner [192]

the intersection between these replicated images used to generate a 3D volumetric representation of the scanned subject. This simplified method led to 30% quantification bias in the lungs and 10–18% in other organs. The quantification bias decreased to 3% through masking the 3D image in the axial direction.

One should note that although transmission-based methods are preferred owing to their higher accuracy, transmission-less strategies are more simple and straightforward to use, less lengthy and more robust to animal motion and registration accuracy. Hence, transmission-less AC is still of interest in preclinical setting, particularly on stand-alone scanners, prototype models or PET/MRI systems not equipped with transmission sources or CT.

Attenuation correction in PET/MRI is more challenging [25, 139]. Although, different strategies are being used on clinical systems, including MRI-based segmentation followed by assignment of predefined attenuation coefficients to segmented regions, atlas-based pseudo-CT generation, joint emission and transmission reconstruction, and more recently deep learning AC approaches [24, 140, 141].

Regarding the small contribution of photon attenuation in small–animal imaging, transmission-less or atlas-based AC methods seem to be the best candidates for preclinical examinations. Since, transmission-less methods ignore the animal bed or other equipment and accessories within the FOV, the use of pre-calculated attenuation maps for animal housing and coils in conjunction with transmission-less methods should provide acceptable accuracy in rodent studies on PET/MRI systems [142].

Scatter correction techniques

Similar to attenuation, Compton scattering is the other central issue in emission tomography that should be addressed to enable quantitative PET analysis. Attenuation compensation without scatter correction (SC) leads to overestimation of tracer uptake within internal organs. The impact of

AC and AC/SC on quantification of tracer uptake in the rat brain was thoroughly investigated by Yu and colleagues [143]. Following AC/SC, ^{18}F-FDG uptake increased in the cerebellum and occipital cortex whereas it decreased in the frontal cortex. In simulation studies carried out by Konik et al., scatter fractions of 4–18% were obtained for different diameters of the whole-body mouse (MOBY) voxelized phantom [131, 144].

Compton scattered events could be generated from either the object or PET scanner's material. The main source of scattering in small animal studies seems to be induced by the scanner's gantry [145, 146]. Relatively larger SFs are reported for scanners with smaller detection rings, larger axial FOVs and dual-layered detector schemes operating with wider energy windows [147]. Intercrystal scattering is another source of scattered photons, which depends upon the crystal density and detector size. As recently demonstrated by Zhang et al., intercrystal scattering becomes significant by increasing the detector size and scintillator density [148].

During the past decade, scanning multiple rodents in one session geared more attention in translational research. Besides high statistical accuracy, imaging several object simultaneously is more efficient in terms of time, cost and throughput, particularly when using short-lived radioisotopes [149]. However, this is at the cost of higher attenuation, scattering and much pronounced parallax errors. In a simulation study carried out by Prasad and Zaidi, ~ 36% and ~ 60% increase in SF was obtained when scanning 3 and 5 MOBY phantoms, respectively, using a 250–650 keV energy window [150], indicating that scatter compensation is of paramount importance for high-throughput quantitative studies. It seems that the new generation of hybrid scanners with advanced correction techniques and dedicated animal chambers will pave the way for simultaneous multi-animal imaging [149].

Various strategies were suggested for Compton scatter correction in small-animal PET imaging, including tail-fitting, multiple-energy windows, convolution subtraction and simulation-based methods including those based on Monte-Carlo or analytical calculations. The former includes Gaussian or quadratic polynomials fitting of the tails of the projection data, which are then subtracted from the total acquired events. Tail-fitting approaches are fast, simple and account for out-of-field scatter as well as Lutetium background radiation. Nevertheless, these techniques are less accurate for correcting scatter within the object since it follows the shape of the curve that best fits the data out of the object boundaries. Multispectral scatter correction methods are among the most promising techniques in SPECT imaging. Improvements in detector technology and energy resolution of PET scanners facilitate the application of these methods in PET studies [151–154]. These approaches are based on estimating the scatter ratio in the photopeak window using the information lying in adjacent energy windows. Although the method accounts for scatter within the object, it fails to recover scattered events generated outside the object boundaries. To tackle this issue, convolution-subtraction methods were introduced to segregate the scattered photons originating from the object, scanner gantry and the detector using the response function extracted from a line source placed at different locations within the scanner's FOV [146, 155]. Although Monte-Carlo simulation provides a more accurate estimate of the distribution of scattered events [156, 157], the majority of PET scanners implement model-based analytical approaches, such as single scatter simulation (SSS), owing to its computational efficiency [158–161].

Model-based methods compute the distribution of single-scattered events using the object's emission and transmission images and then estimate multiple-scattering through a convolution of the estimated single-scattered events with a Gaussian kernel. Prasad and Zaidi compared the scattered profiles of various objects assessed using the SSS algorithm and Monte-Carlo modeling and found a good agreement between the two methods in animal studies [150]. The results of this study indicated the reliability of the SSS algorithm for single and multiple rodents imaging. Comprehensive reviews and comparative assessments of scatter compensation techniques could be found in previous publications by Zaidi and Koral [162–164].

Machine learning methods are witnessed to be much easier and faster than Monte Carlo-based methods and the SSS algorithm in estimating multiple scattered events occurring in PET [140]. These approaches require training to predict the overall scatter contribution or could be used in conjunction with other methods. For instance, one could use the SSS algorithm to compute single-scattered photons followed by estimating multiple-scatter using a trained neural network [140]. However, further investigation is needed to evaluate the accuracy and reliability of these methods for scatter compensation of PET data in preclinical setting.

In closing this section, it should be noted that similar methods are implemented on both clinical and preclinical imaging systems to compensate for physical degrading factors. However, the method of choice strongly depends upon the imaging task, object properties, scanner geometry and the radionuclide used.

Partial volume effect correction

Despite the fast pace of innovation in PET instrumentation and the availability of high-resolution scanners, the quantitative accuracy in PET imaging is negatively influenced by the limited resolution of the scanner [165]. The partial volume effect leads to cross-contamination of tracer uptake among adjacent tissues (spill-over), ultimately leading to substantial quantification bias, particularly in small structures. It is well

known that intricate and tiny structures with approximately twice smaller than PET's spatial resolution (such as the fine details in the brain, the myocardial wall and small tumors or metastasis) are more prone to PVE induced errors [166, 167]. Moreover, other factors, including the background activity, shape and compactness of the structures as well as reconstruction parameters and voxel size, are of paramount importance in the context of PVE.

In response to these concerns, PVE has been addressed through various compensation strategies that could be implemented in both preclinical and clinical emission tomography [168]. In brief, PVE-correction methods could be employed (1) for a particular region-of-interest (region-based (RB) methods) or (2) implemented on the voxel level creating PVE-corrected images (voxel-based (VB) methods).

The simplest RB-technique employs pre-calculated RCs defined as the ratio between the measured and the actual activity concentration. RCs are commonly derived experimentally by scanning a phantom containing spheres of various size surrounded by different levels of activity in the background. The correction procedure consists in choosing the appropriate RC to implement in PET studies depending on objects of similar size and background ratio. Albeit the method is pretty simple and efficient for spherical lesions lying in a homogenous background, it performs poorly in cases with non-uniform tracer uptake or background, which is the case in brain imaging. The geometric transfer matrix (GTM) is an alternative RB PVE-correction method, which requires co-registered high-resolution anatomical images to efficiently segment adjacent regions to several uniform ROIs and finally obtain the signal spread fraction corresponding to each segment. Atlas-based GTM methods have also been investigated on standalone preclinical PET scanners [169].

In comparison to RB methods, VB PVE-correction techniques yield fully PVE-corrected PET images at the voxel level but tend to be more sensitive to noise. Compared to deconvolution-based image restoration, resolution modeling during image reconstruction is more time-consuming but generates more accurate PVE-corrected images with superior noise performance [170]. Moreover, simultaneous implementation of post-reconstruction methods and reconstruction-based methods has shown promising performance in small-animal imaging [171].

Another PVE-correction method that entails structural information was proposed by Bouisson et al. [172]. This multiresolution technique utilizes high-frequency information of MRI or CT images decomposed using the wavelet transform to correct the low-frequency information in emission images.

It is also worth mentioning that most of the reliable PVE-correction approaches are hitherto based on detailed morphological information, which further emphasizes the synergistic strength of hybrid systems toward improved quantification. These methods are more prone to artifacts arising from inaccurate co-registration or where there is a mismatch between the anatomical and functional patterns, thus limiting their practical utility.

Tracer kinetic modeling

Semi-quantitative analysis of PET findings in small rodent studies are conventionally performed using simple image-derived PET metrics from statistic images at a certain time point after tracer injection, including the SUV, percent of injected dose per gram (%ID/g), tumor-to-muscle (or reference tissue) ratios as well as fractional uptake rate (FUR). The limitations of these metrics were reported in previous studies carried out on small laboratory animals [173]. Absolute quantitation in PET imaging is possible through the prism of tracer kinetic modelling, which is being fueled in murine studies by the rapid evolution, and great availability of dedicated high-resolution PET scanners. The mathematical framework linking the measured PET data and the physiological parameters of interest (e.g., metabolic rate of the glucose, blood flow, binding potential) reflecting the tracer behavior in vivo is referred to as the tracer kinetic model, which is doable through compartment modeling.

Compartment modeling is the most frequently used mathematical model to describe a time-variant system through measuring the response of the system to an input function (impulse or Dirac delta function) over time [174]. Therefore, one could model the desired biological system as a single compartment or a combination of several components within which the kinetic states of the tracer are assumed to be equal. The transition of the tracer between the different compartments over time is referred to as rate constant or parameters of the model that could be assessed by means of time activity curves.

Since the measured data in PET imaging are highly affected by inaccuracies from different origins, the derivation of a model relevant to physiological parameters of interest involves several attributes that should be taken into account, including but not limited to, animal preparation, injected activity and mass effect, blood sampling, anesthesia, PET scanner characteristics and the applied corrections.

In quantitative PET imaging, the activity concentration in the arterial blood over a period of time serves as the input function (IF). This can be obtained by serial drawing of blood using manual or automatic blood sampling methods [175]. Although manual sampling is the gold standard technique in human studies, it proved to be the most challenging step in murine studies owing to the intricate vessels and limited blood volume (e.g. ~ 1.5 ml for a 25 gr mice and ~ 25 ml for a 400 gr rat) [176, 177]. Hence, efforts focused on deriving the IF using alternative strategies, such as β-probes (microfluidic chips), which are being used for

direct detection of positrons prior to its annihilation with an electron. As such, it must be in direct contact with the blood to measure the signal emanating from radioactive sources [178, 179]. To minimize the amount of blood loss in previous approaches, arteriovenous-shunt/counter techniques were also proposed in which a catheter is placed in the femoral artery as well as the femoral vein. The blood driven from the artery goes through a coincidence probe and then goes back to the vein [180]. Owing to their invasive nature, these methods are rarely implemented in research studies.

An alternative methodology is image-derived IF. In this method, the IF is extracted from the blood pool voxels in dynamic PET images by defining ROIs on the left ventricular, left atrium or the major vessels, like the ascending aorta [181]. Although the method is non-invasive, it is highly influenced by uncertainties linked to image reconstruction, PVE, motion, scatter, the temporal resolution of the scanner and ROI definition. Hence, for robust and successful measurements, reliable corrections combined with anatomical information should be implemented [169]. As indicated by Evan et al., the GTM-based PV-correction by means of high-resolution MRI information improves the quantitative reliability of TAC curves and image-derived IF in mice heart [182].

Noteworthy, other non-invasive approaches such as reference tissue models, population-based input functions as well as accumulated activity in the bladder or liver have been optimized to derive the IF for small rodents [183–186]. More recently, Kuttner et al. explored two machine learning methods based on Gaussian processes and long short-term memory to estimate the IF from PET/CT images of mice [187]. The IF generated by both models showed good agreement with the image-derived reference arterial IF generated through fitting a well-established model to vena cava and left ventricle of mice PET scan [187].

Another constraint in quantitative small animal PET imaging is related to anesthesia and preconditioning which dramatically alter the kinetic data and confound the final outcome, particularly in neuroimaging or when the muscle tissue serves as reference uptake region [188]. As discussed in the previous section, a dedicated setting and scanning protocol for awake animal imaging was recently suggested, which is applicable to any imaging device [121].

The role of animal handling, preparation and preconditioning is also addressed in the first section. Goetz et al. noticed that optimal heating increases tracer uptake/clearance rate in BALB/c nude mice injected with ^{18}F-Tetrafluoroborate and ^{18}F-FDG [189]. The influence of dietary regime and blood glucose level on ^{18}F-FDG kinetics was also examined in C57BL/6 mice revealing that ^{18}F-FDG uptake rate in different organs depends directly upon the dietary conditions [190]. Regarding the differences in the number of receptors between animals and humans, special attention should be paid to the specific activity of the tracer and amount of injected activity to avoid receptor saturation. In addition to all mentioned factors, the elementary essential role of calibration (dose-calibrator, cross-calibration and all other laboratory instruments being used during the experiments) should not be underestimated.

Last but not least, obtaining comparable, accurate and reproducible results that could be translated to clinical applications is unthinkable without identification, optimization and standardization of factors affecting the outcome.

Summary and future directions

Multi-modality imaging has attracted substantial interest, particularly in the preclinical portfolio. Nevertheless, further research and development efforts still need to be performed to take the full advantage of the quantitative capabilities of small-animal imaging. To this end, achieving optimal image quality and quantitative accuracy involves careful consideration of image acquisition and reconstruction parameters, which need to be standardized for various imaging tasks taking into account the PET scanner's technical specifications, the object under study and properties of the radiotracer, particularly when translation to the clinic is the ultimate goal. Although innovations in hardware are always desired, the new-generation hybrid preclinical scanners will rely on the development of more advanced and modern software solutions for image reconstruction, quantitative corrections, analysis and processing. Automated quantitative solutions, such as atlas-guided techniques will become more popular with the aim of standardizing and minimizing variations across preclinical imaging research facilities [191]. This trend is supported and intensified by ongoing improvements in computational power and increasing role of artificial intelligence and deep learning in biomedical imaging research.

Acknowledgements This work was supported through grant No. 36950 from Tehran University of Medical Sciences and the Swiss National Science Foundation under grant SNSF 320030_176052.

Author contributions MA, HZ and MRA: literature search, literature review, manuscript writing, manuscript editing, content planning.

Compliance with ethical standards

Conflict of interest Mahsa Amirrashedi, Habib Zaidi and Mohammad Reza Ay declare no conflict of interest related to this work.

Ethic standards Ethical approval for producing Fig. 4 was obtained from the Ethics committee of Tehran University of Medical Sciences (Approval ID: IR.TUMS.MEDICINE.REC.1397.004).

References

1. Ma X, Cheng Z (2020) Positron emission tomography (PET) imaging in live animals. In: Tanaka K, Vong K (eds) Handbook of in vivo chemistry in mice: from lab to living system. Wiley, New York, pp 127–149
2. Cal-Gonzalez J, Rausch I, Sundar S, Lalith K, Lassen ML, Muzik O, Moser E, Papp L, Beyer T (2018) Hybrid imaging: instrumentation and data processing. Front Phys 6:47
3. Belcari N, Camarlinghi N, Ferretti S, Iozzo P, Panetta D, Salvadori PA, Sportelli G, Del Guerra A (2017) NEMA NU-4 performance evaluation of the IRIS PET/CT preclinical scanner. IEEE Trans Radiat Plasma Med Sci 1(4):301–309
4. Gu Z, Taschereau R, Vu NT, Prout DL, Silverman RW, Lee JT, Chatziioannou AF (2019) Performance Evaluation of G8, a High-Sensitivity Benchtop Preclinical PET/CT Tomograph. J Nucl Med 60(1):142–149
5. SOFIE (2020) GNEXT PET/CT. https://sofie.com/a-hrefproductsproductsa
6. Szanda I, Mackewn J, Patay G, Major P, Sunassee K, Mullen GE, Nemeth G, Haemisch Y, Blower PJ, Marsden PK (2011) National electrical manufacturers association NU-4 performance evaluation of the PET component of the NanoPET/CT preclinical PET/CT scanner. J Nucl Med 52(11):1741–1747
7. Bruker (2020) Trusted preclinical MR combines with revolutionary PET Performance. https://www.bruker.com/products/preclinical-imaging/nuclear-molecular-imaging
8. Goorden MC, van der Have F, Kreuger R, Ramakers RM, Vastenhouw B, Burbach JPH, Booij J, Molthoff CF, Beekman FJ (2013) VECTor: a preclinical imaging system for simultaneous submillimeter SPECT and PET. J Nucl Med 54(2):306–312
9. MILabs (2020) Preclinical imaging systems. https://www.milabs.com/preclinical-imaging-systems/
10. Del Guerra A, Di Domenico G, Scandola M, Zavattini G (1998) High spatial resolution small animal YAP-PET. Nucl Instrum Methods Phys Res A 409(1–3):537–541
11. Herrmann K, Dahlbom M, Nathanson D, Wei L, Radu C, Chatziioannou A, Czernin J (2013) Evaluation of the Genisys4, a bench-top preclinical PET scanner. J Nucl Med 54(7):1162–1167
12. Nagy K, Tóth M, Major P, Patay G, Egri G, Häggkvist J, Varrone A, Farde L, Halldin C, Gulyás B (2013) Performance evaluation of the small-animal nanoScan PET/MRI system. J Nucl Med 54(10):1825–1832
13. MRSolutions (2020) Preclinical imaging systems. https://www.mrsolutions.com/products/imaging-systems/
14. Magota K, Kubo N, Kuge Y, Nishijima K-i, Zhao S, Tamaki N (2011) Performance characterization of the Inveon preclinical small-animal PET/SPECT/CT system for multimodality imaging. Eur J Nucl Med Mol Imaging 38(4):742–752
15. Sánchez F, Orero A, Soriano A, Correcher C, Conde P, González A, Hernández L, Moliner L, Rodríguez-Alvarez MJ, Vidal L (2013) ALBIRA: a small animal PET/SPECT/CT imaging system. Med Phys 40(5):051906
16. Mediso Medical Imaging Systems (2016) nanoScan SPECT/CT/PET. https://www.mediso.com/products.php?fid=2,11&pid=90
17. MOLECUBES (2020) B-CUBE. https://www.molecubes.com/b-cube/
18. Krishnamoorthy S, Blankemeyer E, Mollet P, Surti S, Van Holen R, Karp JS (2018) Performance evaluation of the MOLECUBES β-CUBE—a high spatial resolution and high sensitivity small animal PET scanner utilizing monolithic LYSO scintillation detectors. Phys Med Biol 63(15):155013
19. Goertzen AL (2004) Development of a combined microPET and microCT system for mouse imaging. University of California Los Angeles, Los Angeles
20. Nicol S, Karkar S, Hemmer C, Dawiec A, Benoit D, Breugnon P, Dinkespiler B, Riviere F, Logier J-P, Niclas M (2009) Design and construction of the ClearPET/XPAD small animal PET/CT scanner. In: 2009 IEEE Nuclear Science Symposium Conference Record (NSS/MIC). IEEE, pp 3311–3314
21. Lage E, Vaquero JJ, Sisniega A, España S, Tapias G, Udías Á, García V, Rodríguez-Ruano A, Desco M (2008) VrPET/CT: development of a rotating multimodality scanner for small-animal imaging. In: 2008 IEEE Nuclear Science Symposium Conference Record. IEEE, pp 4671–4674
22. Cañadas M, Embid M, Lage E, Desco M, Vaquero JJ, Pérez JM (2010) NEMA NU 4–2008 performance measurements of two commercial small-animal PET scanners: ClearPET and rPET-1. IEEE Trans Nucl Sci 58(1):58–65
23. Judenhofer MS, Cherry SR (2013) Applications for preclinical PET/MRI. In: Seminars in nuclear medicine, vol 1. Elsevier, Amsterdam, pp 19–29
24. Cabello J, Ziegler SI (2018) Advances in PET/MR instrumentation and image reconstruction. Br J Radiol 91(1081):20160363
25. Mannheim JG, Schmid AM, Schwenck J, Katiyar P, Herfert K, Pichler BJ (2018) Disselhorst JA PET/MRI hybrid systems. In: Seminars in nuclear medicine, vol 4. Elsevier, Amsterdam, pp 332–347
26. Raylman RR, Majewski S, Lemieux SK, Velan SS, Kross B, Popov V, Smith MF, Weisenberger AG, Zorn C, Marano GD (2006) Simultaneous MRI and PET imaging of a rat brain. Phys Med Biol 51(24):6371
27. Vrigneaud J-M, Mcgrath J, Courteau A, Pegg R, Gomis AS-P, Camacho A, Martin G, Schramm N, Brunotte F (2018) Initial performance evaluation of a preclinical PET scanner available as a clip-on assembly in a sequential PET/MRI system. Phys Med Biol 63(12):125007
28. Lee BJ, Chang C-M, Levin CS (2018) PET system technology designs for achieving simultaneous PET/MRI. In: Iagaru A, Hope T, Veit-Haibach P (eds) PET/MRI in oncology. Springer, Cham, pp 1–26
29. Gonzalez AJ, Berr SS, Cañizares G, Gonzalez-Montoro A, Orero A, Correcher C, Rezaei A, Nuyts J, Sanchez F, Majewski S (2018) Feasibility study of a small animal PET insert based on a single LYSO monolithic tube. Front Med 5:328
30. Goertzen AL, Stortz G, Thiessen JD, Bishop D, Khan MS, Kozlowski P, Retière F, Schellenberg G, Shams E, Sossi V (2016) First results from a high-resolution small animal SiPM PET insert for PET/MR imaging at 7T. IEEE Trans Nucl Sci 63(5):2424–2433
31. Schug D, Lerche C, Weissler B, Gebhardt P, Goldschmidt B, Wehner J, Dueppenbecker PM, Salomon A, Hallen P, Kiessling F (2016) Initial PET performance evaluation of a preclinical insert for PET/MRI with digital SiPM technology. Phys Med Biol 61(7):2851
32. Stortz G, Thiessen JD, Bishop D, Khan MS, Kozlowski P, Retière F, Schellenberg G, Shams E, Zhang X, Thompson CJ (2018) Performance of a PET insert for high-resolution small-animal PET/MRI at 7 tesla. J Nucl Med 59(3):536–542
33. Wu Y, Catana C, Farrell R, Dokhale PA, Shah KS, Qi J, Cherry SR (2009) PET performance evaluation of an MR-compatible PET insert. IEEE Trans Nucl Sci 56(3):574–580
34. Omidvari N, Cabello J, Topping G, Schneider FR, Paul S, Schwaiger M, Ziegler SI (2017) PET performance evaluation of MADPET4: a small animal PET insert for a 7 T MRI scanner. Phys Med Biol 62(22):8671
35. Hallen P, Schug D, Weissler B, Gebhardt P, Salomon A, Kiessling F, Schulz V (2018) PET performance evaluation of the small-animal Hyperion IID PET/MRI insert based on the NEMA NU-4 standard. Biomed Phys Eng Express 4(6):065027

36. Berneking A, Gola A, Ferri A, Finster F, Rucatti D, Paternoster G, Shah NJ, Piemonte C, Lerche C (2018) A new PET detector concept for compact preclinical high-resolution hybrid MR-PET. Nucl Instrum Methods Phys Res A 888:44–52
37. Maramraju SH, Smith SD, Junnarkar SS, Schulz D, Stoll S, Ravindranath B, Purschke ML, Rescia S, Southekal S, Pratte J-F (2011) Small animal simultaneous PET/MRI: initial experiences in a 9.4 T microMRI. Phys Med Biol 56(8):2459
38. CUBRESA (2020) NuPET™ System. https://www.cubresa.com/nupet/
39. Ko GB, Yoon HS, Kim KY, Lee MS, Yang BY, Jeong JM, Lee DS, Song IC, Kim S-k, Kim D (2016) Simultaneous multiparametric PET/MRI with silicon photomultiplier PET and ultra-high-field MRI for small-animal imaging. J Nucl Med 57(8):1309–1315
40. BRIGHTONIX (2019) SimPET™ Simultaneous PET/MRI. https://www.brtnx.com/
41. Inviscan (2018) HALO 3.0 And HALO 2.5 MRI PET Insert. https://www.inviscan.fr/product_pet_mri.html
42. Alexandrakis G, Rannou FR, Chatziioannou AF (2005) Tomographic bioluminescence imaging by use of a combined optical-PET (OPET) system: a computer simulation feasibility study. Phys Med Biol 50(17):4225
43. Prout D, Silverman R, Chatziioannou A (2004) Detector concept for OPET-A combined PET and optical imaging system. IEEE Trans Nucl Sci 51(3):752–756
44. Li C, Yang Y, Mitchell GS, Cherry SR (2011) Simultaneous PET and multispectral 3-dimensional fluorescence optical tomography imaging system. J Nucl Med 52(8):1268–1275
45. Douraghy A, Rannou FR, Silverman RW, Chatziioannou AF (2008) FPGA electronics for OPET: a dual-modality optical and positron emission tomograph. IEEE Trans Nucl Sci 55(5):2541–2545
46. Vanhove C, Bankstahl JP, Krämer SD, Visser E, Belcari N, Vandenberghe S (2015) Accurate molecular imaging of small animals taking into account animal models, handling, anaesthesia, quality control and imaging system performance. EJNMMI Phys 2(1):1–25
47. Reader AJ, Zaidi H (2007) Advances in PET image reconstruction. PET Clin 2(2):173–190
48. Bai B, Asma E (2017) PET image reconstruction: methodology and quantitative accuracy. In: Khalil M (ed) Basic Science of PET Imaging. Springer, Cham, pp 259–284
49. Kinahan PE, Rogers J (1988) Analytic 3D image reconstruction using all detected events. Triumf
50. Shepp LA, Vardi Y (1982) Maximum likelihood reconstruction for emission tomography. IEEE Trans Med Imaging 1(2):113–122
51. Hudson HM, Larkin RS (1994) Accelerated image reconstruction using ordered subsets of projection data. IEEE Trans Med Imaging 13(4):601–609
52. Qi J, Leahy RM, Cherry SR, Chatziioannou A, Farquhar TH (1998) High-resolution 3D Bayesian image reconstruction using the microPET small-animal scanner. Phys Med Biol 43(4):1001
53. Daube-Witherspoon ME, Muehllehner G (1987) Treatment of axial data in three-dimensional PET. J Nucl Med 28(11):1717–1724
54. Defrise M, Kinahan PE, Townsend DW, Michel C, Sibomana M, Newport DF (1997) Exact and approximate rebinning algorithms for 3-D PET data. IEEE Trans Med Imaging 16(2):145–158
55. Lewitt RM, Muehllehner G, Karp JS (1994) Three-dimensional image reconstruction for PET by multi-slice rebinning and axial image filtering. Phys Med Biol 39(3):321
56. Liu X, Defrise M, Michel C, Sibomana M, Comtat C, Kinahan P, Townsend D (1999) Exact rebinning methods for three-dimensional PET. IEEE Trans Med Imaging 18(8):657–664
57. Defrise M, Liu X (1999) A fast rebinning algorithm for 3D positron emission tomography using John's equation. Inverse Probl 15(4):1047
58. Visser EP, Disselhorst JA, Brom M, Laverman P, Gotthardt M, Oyen WJ, Boerman OC (2009) Spatial resolution and sensitivity of the Inveon small-animal PET scanner. J Nucl Med 50(1):139–147
59. Disselhorst JA, Brom M, Laverman P, Slump CH, Boerman OC, Oyen WJ, Gotthardt M, Visser EP (2010) Image-quality assessment for several positron emitters using the NEMA NU 4–2008 standards in the Siemens Inveon small-animal PET scanner. J Nucl Med 51(4):610–617
60. Sato K, Shidahara M, Watabe H, Watanuki S, Ishikawa Y, Arakawa Y, Nai Y, Furumoto S, Tashiro M, Shoji T (2015) Performance evaluation of the small-animal PET scanner ClairvivoPET using NEMA NU 4–2008 standards. Phys Med Biol 61(2):696
61. Bowsher JE, Johnson VE, Turkington TG, Jaszczak RJ, Floyd C, Coleman RE (1996) Bayesian reconstruction and use of anatomical a priori information for emission tomography. IEEE Trans Med Imaging 15(5):673–686
62. Bowsher JE, Yuan H, Hedlund LW, Turkington TG, Akabani G, Badea A, Kurylo WC, Wheeler CT, Cofer GP, Dewhirst MW (2004) Utilizing MRI information to estimate F18-FDG distributions in rat flank tumors. In: IEEE Symposium Conference Record Nuclear Science. IEEE, pp 2488–2492
63. Reader AJ, Verhaeghe J (2014) 4D image reconstruction for emission tomography. Phys Med Biol 59(22):R371
64. Rahmim A, Tang J, Zaidi H (2009) Four-dimensional (4D) image reconstruction strategies in dynamic PET: Beyond conventional independent frame reconstruction. Med Phys 36(8):3654–3670
65. Ralli GP, Chappell MA, Mcgowan DR, Sharma RA, Higgins GS (2018) model with spatial and temporal roughness 4D-PET reconstruction using a spline-residue model with spatial and temporal roughness penalties
66. Gullberg GT, Veress AI, Shrestha UM, Liu J, Ordovas K, Segars WP, Seo Y (2019) Multiresolution spatiotemporal mechanical model of the heart as a prior to constrain the solution for 4D models of the heart. In: 15th International Meeting on Fully Three-Dimensional Image Reconstruction in Radiology and Nuclear Medicine. International Society for Optics and Photonics
67. Ellis S, Reader AJ (2017) Simultaneous maximum a posteriori longitudinal PET image reconstruction. Phys Med Biol 62(17):6963
68. Huisman MC, Reder S, Weber AW, Ziegler SI, Schwaiger M (2007) Performance evaluation of the Philips MOSAIC small animal PET scanner. Eur J Nucl Med Mol Imaging 34(4):532–540
69. Tanaka E, Kudo H (2010) Optimal relaxation parameters of DRAMA (dynamic RAMLA) aiming at one-pass image reconstruction for 3D-PET. Phys Med Biol 55(10):2917
70. Vaissier P, Goorden M, Taylor A, Beekman F (2012) Count-regulated OSEM reconstruction. In: 2012 IEEE Nuclear Science Symposium and Medical Imaging Conference Record (NSS/MIC). IEEE, pp 3315–3320
71. Vaissier PE, Goorden MC, Taylor AB, Beekman FJ (2013) Fast count-regulated OSEM reconstruction with adaptive resolution recovery. IEEE Trans Med Imaging 32(12):2250–2261
72. Goorden MC, van Roosmalen J, van der Have F, Beekman FJ (2016) Optimizing modelling in iterative image reconstruction for preclinical pinhole PET. Phys Med Biol 61(10):3712
73. Gaitanis A, Kastis GA, Vlastou E, Bouziotis P, Verginis P, Anagnostopoulos CD (2017) Investigation of image reconstruction parameters of the mediso nanoscan PC small-animal PET/CT scanner for two different positron emitters under NEMA NU 4–2008 standards. Mol Imaging Biol 19(4):550–559

74. Rahmim A, Qi J, Sossi V (2013) Resolution modeling in PET imaging: theory, practice, benefits, and pitfalls. Med Phys 40 (6Part1)
75. Iriarte A, Marabini R, Matej S, Sorzano COS, Lewitt RM (2016) System models for PET statistical iterative reconstruction: a review. Comput Med Imaging Graph 48:30–48
76. Wang Y, Seidel J, Tsui BM, Vaquero JJ, Pomper MG (2006) Performance evaluation of the GE healthcare eXplore VISTA dual-ring small-animal PET scanner. J Nucl Med 47(11):1891–1900
77. Magdics M, Tóth B, Szécsi L, Csébfalvi B, Szirmay-Kalos L, Szlavecz A, Hesz G, Benyó B, Cserkaszky A, Légrády D (2011) Detector modeling techniques for pre-clinical 3D PET reconstruction on the GPU. Paper presented at the Full 3-D Concerence
78. Mumcuoglu EU, Leahy RM, Cherry SR, Hoffman E (1996) Accurate geometric and physical response modelling for statistical image reconstruction in high resolution PET. In: 1996 IEEE Nuclear Science Symposium. Conference Record. IEEE, pp 1569–1573
79. Panin VY, Kehren F, Michel C, Casey M (2006) Fully 3-D PET reconstruction with system matrix derived from point source measurements. IEEE Trans Med Imaging 25(7):907–921
80. Lyu Y, Lv X, Liu W, Judenhofer MS, Zwingenberger A, Wisner ER, Berg E, McKenney SE, Leung EK, Spencer BA (2019) Mini EXPLORER II: a prototype high-sensitivity PET/CT scanner for companion animal whole body and human brain scanning. Phys Med Biol 64:075004
81. Leroux J-D, Thibaudeau C, Lecomte R, Fontaine R (2007) Fast, accurate and versatile Monte Carlo method for computing system matrix. In: 2007 IEEE Nuclear Science Symposium Conference Record. IEEE, pp 3644–3648
82. Cabello J, Rafecas M (2012) Comparison of basis functions for 3D PET reconstruction using a Monte Carlo system matrix. Phys Med Biol 57(7):1759
83. Camarlinghi N, Sportelli G, Del Guerra A, Belcari N (2018) An automatic algorithm to exploit the symmetries of the system response matrix in positron emission tomography iterative reconstruction. Phys Med Biol 63(19):195005
84. Li K, Safavi-Naeini M, Franklin D, Han Z, Rosenfeld AB, Hutton B, Lerch ML (2015) A new virtual ring-based system matrix generator for iterative image reconstruction in high resolution small volume PET systems. Phys Med Biol 60(17):6949
85. Wang L, Zhu J, Liang X, Niu M, Wu X, Kao C-M, Kim H, Xie Q (2014) Performance evaluation of the Trans-PET® BioCaliburn® LH system: a large FOV small-animal PET system. Phys Med Biol 60(1):137
86. Moehrs S, Defrise M, Belcari N, Del Guerra A, Bartoli A, Fabbri S, Zanetti G (2008) Multi-ray-based system matrix generation for 3D PET reconstruction. Phys Med Biol 53(23):6925
87. Cal-Gonzalez J, Vaquero JJ, Herraiz JL, Pérez-Liva M, Soto-Montenegro ML, Peña-Zalbidea S, Desco M, Udías JM (2018) Improving PET quantification of small animal [68 Ga] DOTA-labeled PET/CT studies by using a CT-based positron range correction. Mol Imaging Biol 20(4):584–593
88. Alva-Sánchez H, Quintana-Bautista C, Martínez-Dávalos A, Ávila-Rodríguez M, Rodríguez-Villafuerte M (2016) Positron range in tissue-equivalent materials: experimental microPET studies. Phys Med Biol 61(17):6307
89. Rodríguez-Villafuerte M, Hernández E, Alva-Sánchez H, Martínez-Dávalos A, Ávila-Rodríguez M (2019) Positron range effects of 66Ga in small-animal PET imaging. Phys Med 67:50–57
90. Bertolli O, Eleftheriou A, Cecchetti M, Camarlinghi N, Belcari N, Tsoumpas C (2016) PET iterative reconstruction incorporating an efficient positron range correction method. Phys Med 32(2):323–330
91. Kotasidis FA, Angelis GI, Anton-Rodriguez J, Matthews JC, Reader AJ, Zaidi H (2014) Isotope specific resolution recovery image reconstruction in high resolution PET imaging. Med Phys 41(5):052503
92. Cal-González J, Herraiz J, España S, Desco M, Vaquero J, Udías JM (2009) Positron range effects in high resolution 3D PET imaging. In: 2009 IEEE Nuclear Science Symposium Conference Record (NSS/MIC). IEEE, pp 2788–2791
93. Bai B, Ruangma A, Laforest R, Tai Y-C, Leahy RM (2003) Positron range modeling for statistical PET image reconstruction. In: 2003 IEEE Nuclear Science Symposium. Conference Record (IEEE Cat. No. 03CH37515). IEEE, pp 2501–2505
94. Herraiz JL, Herranz E, Cal-González J, Vaquero JJ, Desco M, Cussó L, Udias JM (2016) Automatic cardiac self-gating of small-animal PET data. Mol Imaging Biol 18(1):109–116
95. Eleftheriou A, Tsoumpas C, Bertolli O, Stiliaris E (2014) Effect of the magnetic field on positron range using GATE for PET-MR. In: EJNMMI physics, vol S1. Springer, New York
96. Conti M, Eriksson L (2016) Physics of pure and non-pure positron emitters for PET: a review and a discussion. EJNMMI Phys 3(1):8
97. Agoston DV (2017) How to translate time? The temporal aspect of human and rodent biology. Front Neurol 8:92
98. Kotasidis FA, Matthews JC, Angelis GI, Markiewicz PJ, Lionheart WR, Reader AJ (2011) Impact of erroneous kinetic model formulation in Direct 4D image reconstruction. In: 2011 IEEE Nuclear Science Symposium Conference Record. IEEE, pp 2366–2367
99. Cheng X, Bayer C, Maftei C-A, Astner ST, Vaupel P, Ziegler SI, Shi K (2013) Preclinical evaluation of parametric image reconstruction of [18F] FMISO PET: correlation with ex vivo immunohistochemistry. Phys Med Biol 59(2):347
100. Cheng X, Li Z, Liu Z, Navab N, Huang S-C, Keller U, Ziegler SI, Shi K (2015) Direct parametric image reconstruction in reduced parameter space for rapid multi-tracer PET imaging. IEEE Trans Med Imaging 34(7):1498–1512
101. Rahmim A, Tang J, Zaidi H (2013) Four-dimensional image reconstruction strategies in cardiac-gated and respiratory-gated PET imaging. PET Clin 8(1):51–67
102. Rahmim A, Rousset O, Zaidi H (2007) Strategies for motion tracking and correction in PET. PET Clin 2(2):251–266
103. Naseri M, Rajabi H, Wang J, Abbasi M, Kalantari F (2019) Simultaneous respiratory motion correction and image reconstruction in 4D-multi pinhole small animal SPECT. Med Phys 46(11):5047–5054
104. Otani T, Otsuka H, Kondo K, Takizawa H, Nagata M, Kishida M, Miyoshi H (2015) Utility of respiratory-gated small-animal PET/CT in the chronologic evaluation of an orthotopic lung cancer transplantation mouse model. Radiol Phys Technol 8(2):266–277
105. Yang Y, Rendig S, Siegel S, Newport DF, Cherry SR (2005) Cardiac PET imaging in mice with simultaneous cardiac and respiratory gating. Phys Med Biol 50(13):2979
106. Schäfers KP, Lang N, Stegger L, Schober O, Schäfers M (2006) Gated listmode acquisition with the quadHIDAC animal PET to image mouse hearts. Zeitschrift für Medizinische Phys 16(1):60–66
107. Todica A, Lehner S, Wang H, Zacherl MJ, Nekolla K, Mille E, Xiong G, Bartenstein P, la Fougère C, Hacker M (2016) Derivation of a respiration trigger signal in small animal list-mode PET based on respiration-induced variations of the ECG signal. J Nucl Cardiol 23(1):73–83
108. Munoz C, Kolbitsch C, Reader AJ, Marsden P, Schaeffter T, Prieto C (2016) MR-based cardiac and respiratory motion-compensation techniques for PET-MR imaging. PET Clin 11(2):179–191

109. Fayad H, Lamare F, Merlin T, Visvikis D (2016) Motion correction using anatomical information in PET/CT and PET/MR hybrid imaging. Q J Nucl Med Mol Imaging 60(1):12
110. Chun SY, Reese TG, Ouyang J, Guerin B, Catana C, Zhu X, Alpert NM, El Fakhri G (2012) MRI-based nonrigid motion correction in simultaneous PET/MRI. J Nucl Med 53(8):1284–1291
111. Zhong Y, Kalantari F, Zhang Y, Shao Y, Wang J (2018) Quantitative 4D-PET reconstruction for small animal using SMEIR-reconstructed 4D-CBCT. IEEE Trans Radiat Plasma Med Sci 2(4):300–306
112. Ouyang J, Li Q, El Fakhri G (2013) Magnetic resonance-based motion correction for positron emission tomography imaging. In: Seminars in nuclear medicine, vol 1. Elsevier, Amsterdam, pp 60–67
113. Zhou VW, Kyme AZ, Meikle SR, Fulton R (2008) An event-driven motion correction method for neurological PET studies of awake laboratory animals. Mol Imaging Biol 10(6):315–324
114. Kyme AZ, Zhou V, Meikle SR, Fulton RR (2008) Real-time 3D motion tracking for small animal brain PET. Phys Med Biol 53(10):2651
115. Kyme AZ, Zhou VW, Meikle SR, Baldock C, Fulton RR (2011) Optimised motion tracking for positron emission tomography studies of brain function in awake rats. PLoS ONE 6(7):e21727
116. Kyme A, Se S, Meikle S, Angelis G, Ryder W, Popovic K, Yatigammana D, Fulton R (2014) Markerless motion tracking of awake animals in positron emission tomography. IEEE Trans Med Imaging 33(11):2180–2190
117. Zhou V, Eisenhuth J, Kyme A, Akhtar M, Fulton R, Meikle S (2013) A motion adaptive animal chamber for PET imaging of freely moving animals. IEEE Trans Nucl Sci 60(5):3423–3431
118. Miranda A, Staelens S, Stroobants S, Verhaeghe J (2017) Markerless rat head motion tracking using structured light for brain PET imaging of unrestrained awake small animals. Phys Med Biol 62(5):1744
119. Miranda A, Staelens S, Stroobants S, Verhaeghe J (2019) Estimation of and correction for finite motion sampling errors in small animal PET rigid motion correction. Med Biol Eng Comput 57(2):505–518
120. Angelis G, Gillam J, Kyme A, Fulton R, Meikle S (2018) Image-based modelling of residual blurring in motion corrected small animal PET imaging using motion dependent point spread functions. Biomed Phys Eng Express 4(3):035032
121. Kyme AZ, Angelis GI, Eisenhuth J, Fulton RR, Zhou V, Hart G, Popovic K, Akhtar M, Ryder WJ, Clemens KJ (2019) Open-field PET: Simultaneous brain functional imaging and behavioural response measurements in freely moving small animals. Neuroimage 188:92–101
122. Salomon A, Goldschmidt B, Botnar R, Kiessling F, Schulz V (2012) A self-normalization reconstruction technique for PET scans using the positron emission data. IEEE Trans Med Imaging 31(12):2234–2240
123. Badawi RD, Marsden P (1999) Self-normalization of emission data in 3D PET. IEEE Trans Nucl Sci 46(3):709–712
124. Zhang Y, Li H, Baghaei H, Liu S, Ramirez R, An S, Wang C, Wong W-H (2008) A new self-normalization method for PET. J Nucl Med 49(supplement 1):62P–62P
125. de Santana MGC, de Albuquerque Souza GC, Gontijo RMG, Mendes BM, Ferreira AV (2019) Influence of detectors efficiency normalization on small animal PET image quality. Braz J Radiat Sci 7(3)
126. D'Ambrosio D, Zagni F, Spinelli AE, Marengo M (2013) Attenuation correction for small animal PET images: a comparison of two methods. Comput Math Methods Med 2013:103476
127. Prasad R, Ay MR, Ratib O, Zaidi H (2010) CT-based attenuation correction on the FLEX Triumph preclinical PET/CT scanner. IEEE Trans Nucl Sci 58(1):66–75
128. Chow PL, Bai B, Siegel S, Leahy R, Chatziioannou A (2002) Transmission imaging and attenuation correction for the micro-PET/spl reg/P4 tomograph. In: 2002 IEEE Nuclear Science Symposium Conference Record. IEEE, pp 1298–1302
129. Chow PL, Rannou FR, Chatziioannou AF (2005) Attenuation correction for small animal PET tomographs. Phys Med Biol 50(8):1837
130. El Ali HH, Bodholdt RP, Jørgensen JT, Myschetzky R, Kjaer A (2012) Importance of attenuation correction (AC) for small animal PET imaging. Diagnostics 2(4):42–51
131. Konik A, Koesters T, Madsen M, Sunderland J (2011) Evaluation of attenuation and scatter correction requirements as a function of object size in small animal PET imaging. IEEE Trans Nucl Sci 58(5):2308–2314
132. Mayorga Ruiz I (2015) Accuracy of the attenuation correction on small animal PET/CT
133. Hayakawa N, Yamane T, Arias-Loza A-P, Shinaji T, Wakabayashi H, Lapa C, Werner RA, Javadi MS, Pelzer T, Higuchi T (2017) Impact of tissue photon attenuation in small animal cardiac PET imaging. Int J Cardiol 227:257–260
134. Mizuta T, Kitamura K, Iwata H, Yamagishi Y, Ohtani A, Tanaka K, Inoue Y (2008) Performance evaluation of a high-sensitivity large-aperture small-animal PET scanner: ClairvivoPET. Ann Nucl Med 22(5):447–455
135. Pei C, Baotong F, Zhiming Z, Haohui T, Shuangquan L, Xiaoli S, Peilin W, Xiaoming W, Xudong Z, Long W (2019) NEMA NU-4 performance evaluation of a non-human primate animal PET. Phys Med Biol 64(10):105018
136. Bao Q, Newport D, Chen M, Stout DB, Chatziioannou AF (2009) Performance evaluation of the inveon dedicated PET preclinical tomograph based on the NEMA NU-4 standards. J Nucl Med 50(3):401–408
137. Nai Y-H, Ose T, Shidahara M, Watabe H (2017) 137 Cs transmission imaging and segmented attenuation corrections in a small animal PET scanner. Radiol Phys Technol 10(3):321–330
138. Taschereau R, Bao Q, Rannou FR, Chatziioannou AF (2009) Video image based attenuation correction for PETbox, a preclinical PET tomograph. In: 2009 IEEE Nuclear Science Symposium Conference Record (NSS/MIC). IEEE, pp 3350–3352
139. Tsoumpas C, Visvikis D, Loudos G (2016) Innovations in small-animal PET/MR imaging instrumentation. PET Clin 11(2):105–118
140. Gong K, Berg E, Cherry SR, Qi J (2019) Machine learning in PET: from photon detection to quantitative image reconstruction. Proc IEEE 108(1):51–68
141. Mehranian A, Arabi H, Zaidi H (2016) Vision 20/20: magnetic resonance imaging-guided attenuation correction in PET/MRI: challenges, solutions, and opportunities. Med Phys 43(3):1130–1155
142. Evans E, Buonincontri G, Hawkes RC, Ansorge RE, Carpenter TA, Sawiak SJ (2016) Direct evaluation of MR-derived attenuation correction maps for PET/MR of the Mouse Myocardium. IEEE Trans Nucl Sci 63(1):195–202
143. Yu AR, Kim JS, Moon J, Kim HJ, Lim SM, Kim KM (2013) The effect of attenuation and scatter correction in rat brain PET. IEEE Trans Nucl Sci 60(2):751–757
144. Konik AB (2010) Evaluation of attenuation and scatter correction requirements in small animal PET and SPECT imaging
145. Bentourkia Mh, Lecomte R (1999) Energy dependence of non-stationary scatter subtraction-restoration in high resolution PET. IEEE Trans Med Imaging 18(1):66–73
146. Bentourkia M, Msaki P, Cadorette J, Lecomte R (1995) Object and detector scatter-function dependence on energy and position in high resolution PET. IEEE Trans Nucl Sci 42(4):1162–1167
147. Goertzen AL, Bao Q, Bergeron M, Blankemeyer E, Blinder S, Cañadas M, Chatziioannou AF, Dinelle K, Elhami E, Jans H-S

(2012) NEMA NU 4–2008 comparison of preclinical PET imaging systems. J Nucl Med 53(8):1300–1309
148. Zhang C, Sang Z, Wang X, Zhang X, Yang Y (2019) The effects of inter-crystal scattering events on the performance of PET detectors. Phys Med Biol 64(20):205004
149. Greenwood HE, Nyitrai Z, Mocsai G, Hobor S, Witney TH (2019) High throughput PET/CT imaging using a multiple mouse imaging system. J Nucl Med 61(2):292–297
150. Prasad R, Zaidi H (2014) Scatter characterization and correction for simultaneous multiple small-animal PET imaging. Mol Imaging Biol 16(2):199–209
151. Adam L-E, Karp JS, Freifelder R (2000) Energy-based scatter correction for 3-D PET scanners using NaI (Tl) detectors. IEEE Trans Med Imaging 19(5):513–521
152. Grootoonk S, Spinks T, Sashin D, Spyrou N, Jones T (1996) Correction for scatter in 3D brain PET using a dual energy window method. Phys Med Biol 41(12):2757
153. Grootoonk S, Spinks T, Jones T, Michel C, Bol A (1991) Correction for scatter using a dual energy window technique with a tomograph operated without septa. In: Conference Record of the 1991 IEEE Nuclear Science Symposium and Medical Imaging Conference. IEEE, pp 1569–1573
154. Bendriem B, Trebossen R, Frouin V, Syrota A (1993) A PET scatter correction using simultaneous acquisitions with low and high lower energy thresholds. In: 1993 IEEE Conference Record Nuclear Science Symposium and Medical Imaging Conference. IEEE, pp 1779–1783
155. Bentourkia M, Msaki P, Cadorette J, Lecomte R (1996) Nonstationary scatter subtraction-restoration in high-resolution PET. J Nucl Med 37(12):2040
156. Zaidi H, Scheurer AH, Morel C (1999) An object-oriented Monte Carlo simulator for 3D cylindrical positron tomographs. Comput Methods Programs Biomed 58(2):133–145
157. Levin CS, Dahlbom M, Hoffman EJ (1995) A Monte Carlo correction for the effect of Compton scattering in 3-D PET brain imaging. IEEE Trans Nucl Sci 42(4):1181–1185
158. Watson CC (2000) New, faster, image-based scatter correction for 3D PET. IEEE Trans Nucl Sci 47(4):1587–1594
159. Werling A, Bublitz O, Doll J, Adam L-E, Brix G (2002) Fast implementation of the single scatter simulation algorithm and its use in iterative image reconstruction of PET data. Phys Med Biol 47(16):2947
160. Ollinger JM (1996) Model-based scatter correction for fully 3D PET. Phys Med Biol 41(1):153
161. Watson CC, Newport D, Casey ME (1996) A single scatter simulation technique for scatter correction in 3D PET. Three-dimensional image reconstruction in radiology and nuclear medicine, vol 4. Springer, Dordrecht, pp 255–268
162. Zaidi H (2001) Scatter modelling and correction strategies in fully 3-D PET. Nucl Med Commun 22(11):1181–1184
163. Zaidi H (2000) Comparative evaluation of scatter correction techniques in 3D positron emission tomography. Eur J Nucl Med 27(12):1813–1826
164. Zaidi H (2004) Koral K (2004) Scatter modelling and compensation in emission tomography. Eur J Nucl Med Mol Imaging 31:761–782
165. Cysouw MC, Kramer GM, Schoonmade LJ, Boellaard R, De Vet HC, Hoekstra OS (2017) Impact of partial-volume correction in oncological PET studies: a systematic review and meta-analysis. Eur J Nucl Med Mol Imaging 44(12):2105–2116
166. Cal-González J, Tsoumpas C, Lassen M, Rasul S, Koller L, Hacker M, Schäfers K, Beyer T (2017) Impact of motion compensation and partial volume correction for 18F-NaF PET/CT imaging of coronary plaque. Phys Med Biol 63(1):015005
167. Turco A, Nuyts J, Duchenne J, Gheysens O, Voigt J-U, Claus P, Vunckx K (2017) Analysis of partial volume correction on quantification and regional heterogeneity in cardiac PET. J Nucl Cardiol:1–9.
168. Bettinardi V, Castiglioni I, De Bernardi E, Gilardi M (2014) PET quantification: strategies for partial volume correction. Clin Transl Imaging 2(3):199–218
169. Lehnert W, Gregoire M-C, Reilhac A, Meikle SR (2012) Characterisation of partial volume effect and region-based correction in small animal positron emission tomography (PET) of the rat brain. Neuroimage 60(4):2144–2157
170. Hoetjes NJ, van Velden FH, Hoekstra OS, Hoekstra CJ, Krak NC, Lammertsma AA, Boellaard R (2010) Partial volume correction strategies for quantitative FDG PET in oncology. Eur J Nucl Med Mol Imaging 37(9):1679–1687
171. Cal-González J, Moore S, Park M, Herraiz J, Vaquero J, Desco M, Udias J (2015) Improved quantification for local regions of interest in preclinical PET imaging. Phys Med Biol 60(18):7127
172. Boussion N, Hatt M, Lamare F, Bizais Y, Turzo A, Cheze-Le Rest C, Visvikis D (2006) A multiresolution image based approach for correction of partial volume effects in emission tomography. Phys Med Biol 51(7):1857
173. Prando S, Carneiro CdG, Robilotta CC, Sapienza MT (2019) Comparison of different quantification methods for 18F-fluorodeoxyglucose-positron emission tomography studies in rat brains. Clinics 74:e1273
174. Morris ED, Endres CJ, Schmidt KC, Christian BT, Muzic RF, Fisher RE (2004) Kinetic modeling in positron emission tomography. Emission tomography: The Fundamentals of PET and SPECT. Academic Press, San Diego
175. Kuntner C (2014) Kinetic modeling in pre-clinical positron emission tomography. Zeitschrift für Med Phys 24(4):274–285
176. Laforest R, Sharp TL, Engelbach JA, Fettig NM, Herrero P, Kim J, Lewis JS, Rowland DJ, Tai Y-C, Welch MJ (2005) Measurement of input functions in rodents: challenges and solutions. Nucl Med Biol 32(7):679–685
177. Riches A, Sharp JG, Thomas DB, Smith SV (1973) Blood volume determination in the mouse. J Physiol 228(2):279–284
178. Liu Z, Lan X (2019) Microfluidic radiobioassays: a radiometric detection tool for understanding cellular physiology and pharmacokinetics. Lab Chip 19(14):2315–2339
179. Maneuski D, Giacomelli F, Lemaire C, Pimlott S, Plenevaux A, Owens J, O'Shea V, Luxen A (2017) On the use of positron counting for radio-assay in nuclear pharmaceutical production. Appl Radiat Isot 125:9–14
180. Alf MF, Wyss MT, Buck A, Weber B, Schibli R, Krämer SD (2013) Quantification of brain glucose metabolism by 18F-FDG PET with real-time arterial and image-derived input function in mice. J Nucl Med 54(1):132–138
181. Watabe W, Channing MA, Riddell C, Jousse F, Libutti SK, Carrasquillo JA, Bacharach SL, Carson RE (2001) Noninvasive estimation of the aorta input function for measurement of tumor blood flow with [/sup 15/O] water. IEEE Trans Med Imaging 20(3):164–174
182. Evans E, Buonincontri G, Izquierdo D, Methner C, Hawkes RC, Ansorge RE, Krieg T, Carpenter TA, Sawiak SJ (2015) Combining MRI with PET for partial volume correction improves image-derived input functions in mice. IEEE Trans Nucl Sci 62(3):628–633
183. Bertoglio D, Verhaeghe J, Korat Š, Miranda A, Stroobants S, Mrzljak L, Dominguez C, Liu L, Skinbjerg M, Munoz-Sanjuan I (2019) In vitro and in vivo assessment of suitable reference region and kinetic modelling for the mGluR1 Radioligand [11 C] ITDM in Mice. Mol Imaging Biol:1–10
184. Meyer M, Le-Bras L, Fernandez P, Zanotti-Fregonara P (2017) Standardized input function for 18F-FDG PET studies in mice: a cautionary study. PLoS ONE 12(1):e0168667

185. Wong K-P, Zhang X, Huang S-C (2013) Improved derivation of input function in dynamic mouse [18 F] FDG PET using bladder radioactivity kinetics. Mol Imaging Biol 15(4):486–496
186. Ye Q, Lyu Z, Yao S, Dong Y, Liu H, Wu J, Liu Y, Ma T (2018) Direct 4D Patlak Reconstruction in Dynamic FDG PET Imaging with Population-based Input Function. In: 2018 IEEE Nuclear Science Symposium and Medical Imaging Conference Proceedings (NSS/MIC). IEEE, pp 1–4
187. Kuttner S, Wickstrøm KK, Kalda G, Dorraji SE, Martin-Armas M, Oteiza A, Jenssen R, Fenton K, Sundset R, Axelsson J (2020) Machine learning derived input-function in a dynamic 18F-FDG PET study of mice. Biomed Phys Eng Express 6(1):015020
188. Bascuñana P, Thackeray JT, Bankstahl M, Bengel FM, Bankstahl JP (2019) Anesthesia and preconditioning induced changes in mouse brain [18 F] FDG uptake and kinetics. Mol Imaging Biol 21(6):1089–1096
189. Goetz C, Podein M, Braun F, Weber WA, Choquet P, Constantinesco A, Mix M (2017) Influence of animal heating on PET imaging quantification and kinetics: biodistribution of 18F-tetrafluoroborate and 18F-FDG in Mice. J Nucl Med 58(7):1162–1166
190. Wong K-P, Sha W, Zhang X, Huang S-C (2011) Effects of administration route, dietary condition, and blood glucose level on kinetics and uptake of 18F-FDG in mice. J Nucl Med 52(5):800–807
191. Gutierrez DF, Zaidi H (2012) Automated analysis of small animal PET studies through deformable registration to an atlas. Eur J Nucl Med Mol Imaging 39(11):1807–1820
192. Amirrashedi M, Sarkar S, Ghafarian P, Hashemi Shahraki R, Geramifar P, Zaidi H, Ay MR (2019) NEMA NU-4 2008 performance evaluation of Xtrim-PET: A prototype SiPM-based preclinical scanner. Med Phys 46(11):4816–4825